Ice aprons on steep high-alpine slopes: insights from the Mont-Blanc massif, Western Alps

Ludovic Ravanel[1,2] , Grégoire Guillet[3] , Suvrat Kaushik[1,4],

Susanne Preunkert[5], Emmanuel Malet[1], Florence Magnin[1], Emmanuel Trouvé[4],

Maurine Montagnat[5] , Yajing Yan[4] and Philip Deline[1]

[1]EDYTEM, Université Savoie Mont-Blanc, CNRS (UMR 5204), 73370 Le Bourget du Lac, France; [2]Department of Geosciences, University of Oslo, Sem Sælands vei 1, 0371 Oslo, Norway; [3]School of Geography & Sustainable Development, University of St Andrews, St Andrews KY16 9AL, UK; [4]LISTIC, Université Savoie Mont Blanc, Polytech, 74944 Annecy-le-Vieux, France and [5]IGE, Université Grenoble Alpes, CNRS (UMR 5001), 38000 Grenoble, France

Abstract

Ice aprons are defined as very small ice bodies covering steep rock slopes. They have only been the subject of increased scientific interest for a few years, despite the fact that they are a condition for mountaineering and obvious elements in the high-alpine landscapes. However, very little is known about their distribution, evolution and physical characteristics. In this paper, we review the existing knowledge on ice aprons, which have almost exclusively been investigated in the Mont-Blanc massif, Western Alps. We supplement this review with novel results from recent surveys of ice aprons. We used a wide array of methodologies, from remote sensing (multi-source imagery) to in situ (stakes and thermal monitoring) and laboratory (radiocarbon dating and texture analysis) glaciological investigations. In the Mont-Blanc massif, ice aprons occupy $4.2 \, \text{km}^2$ within the alpine permafrost zone. Temperature measured at the ice–rock interface is indeed largely negative. Thinness of ice aprons coupled with the cold context implies a quasi-stationary shear regime without basal Sliding. Only ice at the surface can possibly melt in warm periods. After a shrinking period from the end of the Little Ice Age to the mid-to-late-1960s, ice aprons experienced a short period of expansion, followed by an accelerated shrinkage since the beginning of the 21st century. This shrinkage now favours rockfall triggering and poses a serious threat to a glaciological heritage since ice aprons host several-thousand-year-old ice. Finally, we synthesize this information to assess the existing definition of ice aprons, and propose some future research directions.

1. Introduction

Definitions of ice aprons (IAs hereafter) are often conflicting. IAs have been defined as 'thin mass of snow and ice adhering to a mountainside' by Armstrong and others (1973). Bhutiyani (2011) states that IAs are 'small accumulations of snow and ice, generally found above the equilibrium line, that stick to the topography of the glacierized basin'. Among mountain glaciers constrained by the topography, Benn and Evans (2010) identify a group related to the smallest glaciers with: (1) *glacierets* that are thin ice patches produced by snowdrifting and avalanching and occupying depressions on low-angle terrains; (2) *niche glaciers* that are ice bodies, undergoing significant movement, whose location is controlled by a niche or rock bench in a mountain or valley side and (3) *ice aprons* that are 'thin snow and ice accumulations adhering to mountainsides' (Fig. 1), to which they add *snow patches*. For Cogley and others (2011), IA is synonymous to 'mountain apron glacier'. This definition conflicts with the previously stated ones over the dynamics of IAs (flowing glaciers vs non-flowing IAs). Guillet and Ravanel (2020) further defined IAs where gravity-driven mass transfer is considered to be negligible. IAs are thus defined as 'very small (typically <0.1 km²) ice bodies of irregular outline, lying on slopes >40°, regardless of whether they are thick enough to significantly deform under their own weight'. This definition covers IAs in all types of high-alpine north faces (see Figs 1, 2) and will be further used here and completed or corrected if necessary.

Within the mountaineering community, the north faces of Matterhorn (4478 m a.s.l., Valais Alps, Switzerland), Grandes Jorasses (4208 m, Mont-Blanc massif, France), Eiger (3967 m, Bernese Oberland, Switzerland) and Drus (3754 m, Mont-Blanc massif, France) are known – due to their difficulty and height – as the 'four great north faces of the alps'. These steep rock faces participate in the alpine myth (Raffestin, 2001) through the high-mountain landscapes to which they contribute with more or less large IAs. These ice bodies are permanently present in many north faces located above 3000/3500 m a.s.l. in the alps and sometimes on sunnier slopes at higher altitudes (e.g. Italian side of Mont Blanc, 4808 m a.s.l.). Over the last century and a half, several IAs in the Mont-Blanc massif (MBM) have recorded drastic surface area loss, with an increase in melting rates since the 1990s. Recent melt became more and more visible thanks to the disconnection between current ice surfaces and past in situ mountaineering equipment, as well as the emergence of rock spurs within IAs. This evolution not only contributes to changing the high-alpine landscapes
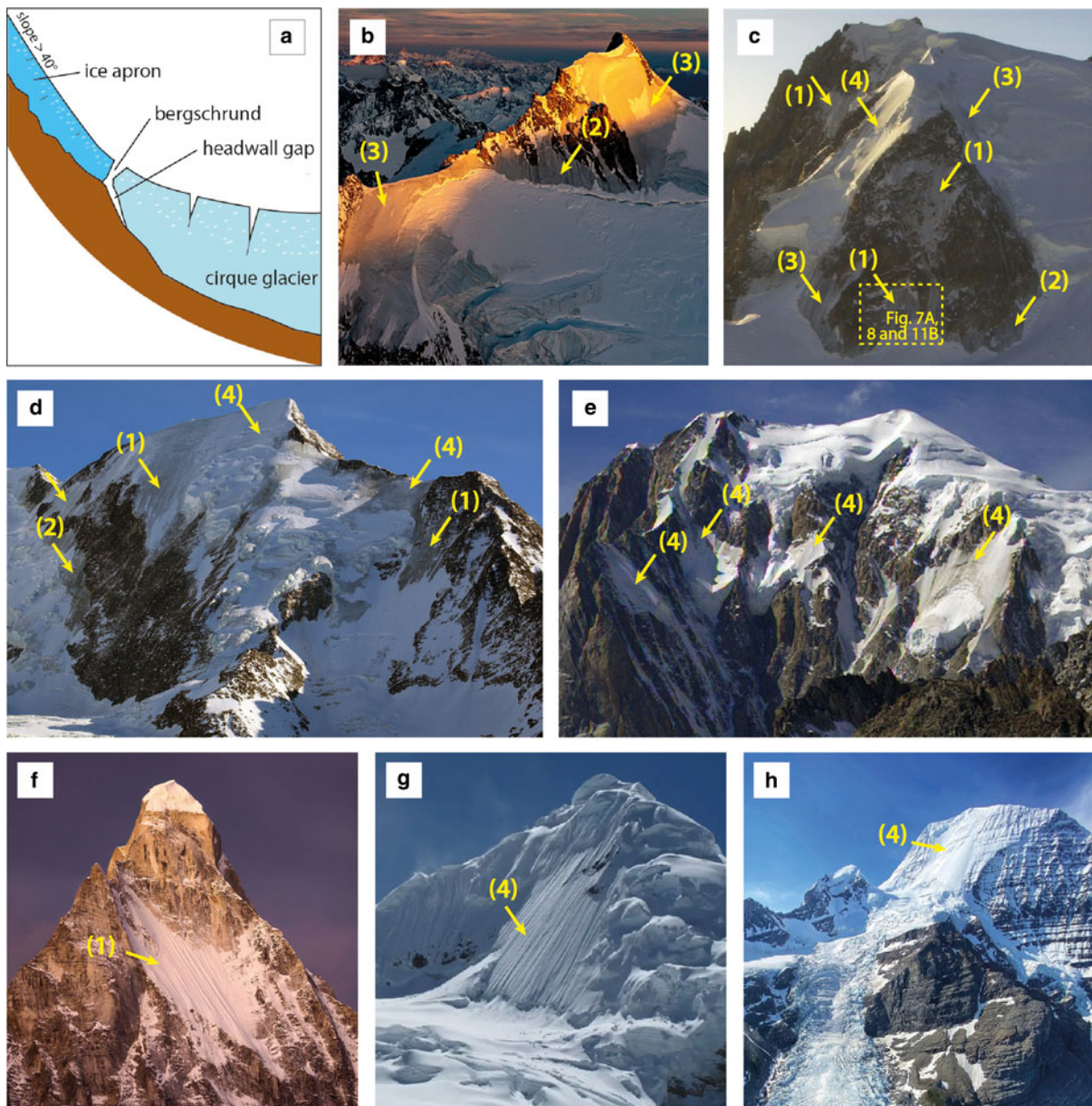
Fig. 1. IAs. (a) Sketch (cross section) of an IA overlooking a cirque glacier. IAs are present in different contexts, as in the MBM; (b) west face of Mont Maudit (4465 m a.s.l.); (c) north face of Mont Blanc du Tacul (4248 m) with its rocky Triangle (3970 m); (d) north face of Aiguille de Bionnassay (4052 m); (e) east face of Mont Blanc (4808 m). IAs are present in many high-altitude mountain ranges: (f) north face of Shivling (6543 m, Garhwal Himalaya, India; photo: A. Upadhya); (g) west face of Tocllaraju (6034 m a.s.l.; Cordillera Blanca, Peruvian Andes; photo: N. Heald); (h) Mount Robson (3954 m, Canadian Rockies; photo: B. Derek). Yellow arrows indicate IAs. Numbers correspond to different contexts (see Section 3.2): (1) 'long-standing exposed' IA; (2) IA previously buried under the ice of another glacier (on B: thickness reduction of one of the tributaries of Bossons Glacier; on D: shrinkage of Bionnassay Glacier revealed several tens of metres high slopes); (3) quasi-continuous IA; (4) IAs overlooking hanging, slope or cirque glaciers.

Fig. 2. Typology of the high-alpine north faces according to Galibert ([1965](#)) excluding slopes with thick mobile glacier like avalanching glaciers or ice falls. (a) North face with almost continuous ice/snow cover – Trugberg north ridge (3933 m a.s.l., Bernese Alps, Switzerland) with its north (left) and west (right) faces (photo: September 2018); (b) mixed north face – Mönch north face (4107 m, Bernese Alps, Switzerland) (photo: S. Rasanen, August 2012); (c) north rock face partly covered by ice – Jungfrau northwest face (4158 m, Bernese Alps, Switzerland) (photo: B. Tibbetts, March 2018).

– which are becoming darker and darker by losing ice and snow (Moreau, 2010) – but also challenges the traditional practice of mountaineering which has used these IAs as access routes to summits for more than a century. Rébuffat (1973) – a French mountain guide who was the first to climb all four of the great north faces – published a collection of the 100 most beautiful mountaineering routes of the MBM. In total, 50% of them include IAs, and recent changes make the climbs more technically challenging and dangerous (Mourey and others, 2019). In terms of difficulty, this results today in steeper IAs, with predominant ice surface while they were generally covered with snow until the early 2000s, requiring advanced ice climbing skills. In addition, the retreat of IAs is likely to trigger rockfalls, endangering mountaineers within their vicinity. Given their very small dimensions, the effects of the IA vanishing on water availability and ecology are minimal. Interest in IAs is however renewed today because of (1) the current and future impacts of their evolution on mountaineering, (2) their relation with, and impact on the underlying permafrost and rockfall hazards associated with its degradation/ warming and (3) the profound lack of fundamental knowledge.

Despite the absence of widespread and systematic surveys, IAs are very frequent in high-alpine mountain areas like the Andes, Rockies, Himalaya or European Alps (Fig. 1). Nonetheless, IAs have so far received relatively poor attention since the works of Galibert (1960b, 1965) that documented IAs in three types of north faces (excluding slopes with thick mobile glaciers) (Fig. 2):

(1) the faces with quasi-continuous 'snow/ice shells' (Galibert, 1965). Their almost immobility without any crevasses distinguishes them from crevassed and mobile slope glaciers (Galibert, 1960a). However, very slight movements can in places be revealed by cracks visible on the surface. The author notes that, in the case of Trugberg (3933 m a.s.l., Bernese Alps, Switzerland, Fig. 2a), the layer of snow covering the ice was 2- (top part) to 15 m thick (lower part) with coarse-grained snow beds alternating with layers of ice. Deeper, the snow was giving way to massive ice until bedrock.
(2) The mixed north faces where large sectors of bare rock contrast with the 'ice/snow filling couloirs and hollows'. The thickness of the fillings typically varies from 3 to 5 m, and their distribution is likely to be related to rock structures enabling snow deposition and ice formation in the most fractured areas. Galibert (1965) gives the north face of Mönch (4107 m a.s.l., Bernese Alps, Switzerland; Fig. 2b) as an example.
(3) The sub-vertical rock faces with 'high-altitude ice covers'. Few north faces culminating above 4000 m a.s.l. are rocky up to their summit (Galibert, 1960b). Only slopes >70° seem to exclude the formation of ice cover. Such rock walls are strongly inclined and, in a more or less discontinuous manner, can be covered with sparse, thin ice patches whose formation is favoured, as in the case of the northwest face of Jungfrau (4158 m a.s.l., Bernese Alps, Switzerland; Fig. 2c), by the horizontal component of the rock structure (small ledges on which snow and ice accumulate).

This typology also highlights the difficulty of precisely defining these small ice bodies and the necessity to differentiate them from other cryospheric bodies lying on steep slopes: thick mobile glaciers/icefalls (Benn and Evans, 2010) and avalanching glaciers such as cold-based hanging glaciers (Flotron, 1977; Pralong and Funk, 2006; Margreth and others, 2011).

The origin of IAs, their evolution with time and climate and their relationships with other high-mountain cryospheric bodies in their vicinity (permafrost, hanging glaciers, etc.) remain to be explored. This paper reviews the existing knowledge on IAs,

entirely carried out in the MBM. We will first evoke recently published remote sensing, modelling and statistical methods used to study IAs, before discussing the already published evolution of IAs since the end of the Little Ice Age (LIA, about 1850 CE). We then present in detail new complementing results of two on-site sensor arrays used for IA thermal monitoring. In addition, already published ice texture analysis and radiochemical dating from ice cores are presented. According to the reported ice texture and age dating, we also discuss the dynamic regime and the depth/age relationship for ice in IAs.

2. Study area: the Mont-Blanc massif

The MBM covers an area of 550 km^2 in the north-western European Alps (Fig. 3). It is predominantly composed of a heavily fractured crystalline basement formed by a granitic body intruding through metamorphic series (Bertini and others, 1985; Bussy and von Raumer, 1994). In total, 28 of the 82 summits ⩾4000 m a.s.l. in the alps are located in the MBM, forming the drainage divide between the Rhône and Po basins. Permafrost or perennially frozen ground (Harris and others, 2009) is present throughout a large area: modelled as 'possible', 'likely' and 'almost certain', permafrost covers 79, 65 and 45% of the 86 km^2 of rock walls steeper than 40° on the French side of the MBM, respectively (Magnin and others, 2015a). Research carried out on steep permafrost-affected slopes of the MBM has in particular made it possible to show the relationship between global warming and slope instabilities (e.g. Ravanel and Deline, 2011) before showing the role of warming permafrost within bedrock in rockfall triggering (e.g. Ravanel and others, 2017a, 2017b; Legay and others, 2021). Next to topography and geological structure, ice-related permafrost conditions and topographic history including glacier vanishing are of primary importance in explaining rockfall occurrences. The formation and persistence of permafrost is driven by the cold mean annual air temperatures characteristic of high-altitude areas. In the MBM, the 0°C isotherm is situated from 2200 on the north side to 2700 m a.s.l. on the south side (Durand and others, 2009). At the Aiguille du Midi (3842 m a.s.l.), the mean annual temperature is ∼−7.8°C (Magnin and others, 2015b). These low temperatures are also very likely a condition for the presence and persistence of cold IAs (Haeberli, 1975).

Excluding small (typically <0.5 km^2) ice masses such as IAs, ∼30% (155 km^2) of the MBM area is covered by 94 glaciers including 12 with a surface area >5 km^2 (Gardent and others, 2014; Berthier and others, 2016; see Fig. 3). The accumulation zone of some of these glaciers exceeds 4000 m a.s.l., and their related fronts can reach down to ∼1500 m a.s.l. The flow of the MBM glaciers has been the subject of numerous in situ or remotely sensed velocity measurements (e.g. Gagliardini and Meyssonnier, 1997; Berthier and others, 2005; Fallourd and others, 2011) in order to better characterize the dynamics of warm- and cold-based glaciers (Pourchet and others, 1998; Suter and Hoelzle, 2002), with particular emphasis on hazard assessment (e.g. Le Meur and Vincent, 2006; Margreth and others, 2011; Dematteis and others, 2021). Glaciological field measurements are performed routinely on several glaciers, including the Mer de Glace and Argentière Glacier (e.g. Six and Vincent, 2014). This massif has also proved appropriate for evaluating new remote-sensing techniques (e.g. Berthier and others, 2005, 2014). The recent decline of the MBM glaciers has been abundantly quantified from field data (e.g. Vallon and others, 1998; Vincent, 2002; Vincent and others, 2009) and remote-sensing methods (e.g. Vernier and others, 2011; Berthier and others, 2014; Gardent and others, 2014; Dehecq and others, 2016; Réveillet and others, 2021) but very few studies have focused on IAs.
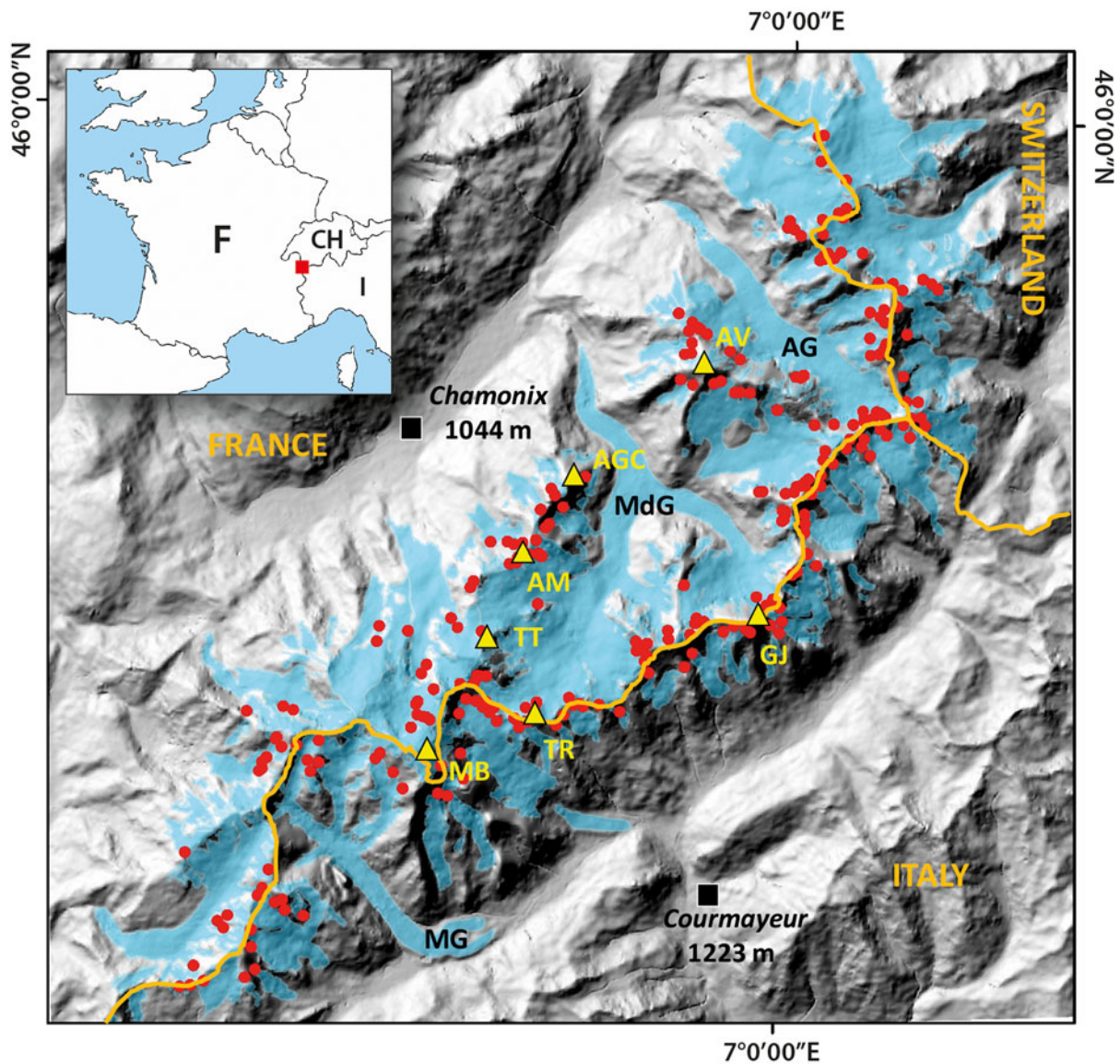
Fig. 3. IAs of the MBM (background: ASTER DEM). In blue: glacier outlines (2019); red dots: IAs; yellow triangles: summits. MB: Mont Blanc (4808 m a.s.l.); AM: Aiguille du Midi (3842 m); TT: Triangle du Tacul (3970 m); TR: Tour Ronde (3792 m; sampling site for dating); AGC: Aiguille des Grands Charmoz (3445 m); GJ: Grandes Jorasses (4208 m); AV: Aiguille Verte (4122 m); MG: Miage Glacier; MdG: Mer de Glace; AG: Argentière Glacier. Elevations are in m a.s.l.; yellow line: national boundaries.

3. Characteristics of current ice aprons

IAs are small, but they are likely to settle in many areas as long as the snow can accumulate and be preserved enough to form ice. Given the slope of the IAs which is unfavourable to thick accumulations of snow, it should be noted that the formation of ice does not occur by compressive firnification metamorphosis but more likely by refreezing of meltwater in snow in the same way as superimposed ice in perennial ice patches (Davesne and others, 2022). The study of Kaushik and others (2022a) carried out at the scale of the whole MBM made it possible to specify the spatial distribution of IAs, resulting in a better understanding of their location within the high-mountain slopes as well as their relations with the other types of glaciers.

3.1. Distribution of ice aprons

A combination of very high-spatial resolution images like the orthophotos available from www.geoportail.gouv.fr (0.4 m resolution), panchromatic images from SPOT 6 (1.5 m resolution) and the high-resolution images available from Google Earth

were accurately used in order to manually digitize IAs in the MBM under a GIS environment (Kaushik and others, 2021, 2022a). Since IAs have a slope >40° (slope angle regularly used as a minimum value to define rock walls), they might be confused with avalanching glaciers but they do not have a vertical front from which blocks of ice ('séracs') break off, nor do they have crevasses. The upper boundary of an IA is generally indicated by the ice–rock transition. The lower boundary is either marked by such an ice–rock transition (when IA is located within a rock face) or by a bergschrund (when the IA stands on top of a glacier of a different type; see Schweizer, 1988) (see e.g. Fig. 9), i.e. a crevasse that forms between the relatively stable IAs and the more mobile glacier downstream.

A total of 423 IAs were identified by Kaushik and others (2022a) (Fig. 3), corresponding to a total of 4.21 km^2 which is ~0.8% of the massif surface area and ~2.6% of the total surface area covered by ice (162.4 km^2 according to Kaushik and others, 2022a). Regarding the surface area of IAs, the statement of Guillet and Ravanel (2020) defining IA <0.1 km^2 is confirmed since the values in the MMB are from 0.001 to 0.05 km^2. This upper limit does not seem restricted to the MMB since very

large IAs like the main one on the Shivling north face (6543 m a.s.l.; Garhwal Himalaya, India; Fig. 1f) or on the west face of Tocllaraju (6034 m a.s.l.; Cordillera Blanca, Peruvian Andes; Fig. 1g) have a surface area ~0.1 km². Problems associated with the lack of coverage over the entire MBM, presence of cloud cover, illumination and shadow area issues, which make visual interpretation difficult and the presence of seasonal snow cover were all overcome using images acquired through different modes (Kaushik and others, 2022a).

According to the same authors, 87.5% of IAs are located above 3100 m a.s.l. (Fig. 4a), i.e. above the regional equilibrium line altitude (Rabatel and others, 2013). The lowest ice bodies are generally located at the foot of cold north faces. IAs are present in all orientations (Fig. 4b) with a maximum on northwest faces (19.4%), then north (16.3%) and, counter-intuitively, south (14.4%), where the IAs are located at higher altitude than the north-facing IAs. In total, 58% of the IAs have a slope angle between 50° and 65° (Fig. 4c) like IAs of Triangle du Tacul, Tour Ronde or Grandes Jorasses. For some, slopes are >75°. Comparable work outside the MBM and the alps is necessary to validate and complete the results of this first regional survey, in particular to verify the relative part of IAs within the ice-covered areas.

3.2. Four types of occurrence of ice aprons

To better understand the location of IAs on rock walls and their spatial relationships with glaciers, four types of IA formation contexts can be observed in the MBM based on the survey of Kaushik and others (2022a):

(1) type 1 is 'long-standing exposed' IAs ((1) in Fig. 1), i.e. IAs having continuously existed independently of any glacier outside ice ages; they are overall receding (Section 4.1);
(2) the retreat of glacier bodies releases IAs possibly previously buried under the ice (type 2), including at very high altitudes (Fig. 1b); for example, retreat of valley or slope glaciers frees sectors at the foot of steep back-walls ((2) in Figs 1b, c), or lateral rock slopes on which ice remains ((2) in Fig. 1d);
(3) type 3 corresponds to an evolution of what Galibert (1965) called 'north faces with quasi-continuous snow/ice shells': these pretty steep slopes that used to be snow-covered all year long become steeper as the snow and then the ice melt; the surface of the IA is then completely freed from snow, temporarily or permanently ((3) in Fig. 1);
(4) type 4 corresponds to IAs that overlook hanging, slope or cirque glaciers; these IAs tend to lose their snow cover; it often allows the distinction between steep IAs ((4) in Figs 1b, c) and glaciers, the latter being gentler, snow-covered and whose mobility is shown by crevasses.

4. Evolution of ice aprons at different timescales and related geomorphological effects

Since the 1980s, the glaciers in the alps displayed a general shrinkage (e.g. Paul and others, 2011; Gardent and others, 2014) as documented in most mountain ranges worldwide (e.g. Roe and others, 2017; Hugonnet and others, 2021). In this context, the accurate quantification of changes in IAs through surface area reconstruction was needed to better understand IAs/climate relationships. Although some international glacier inventories have
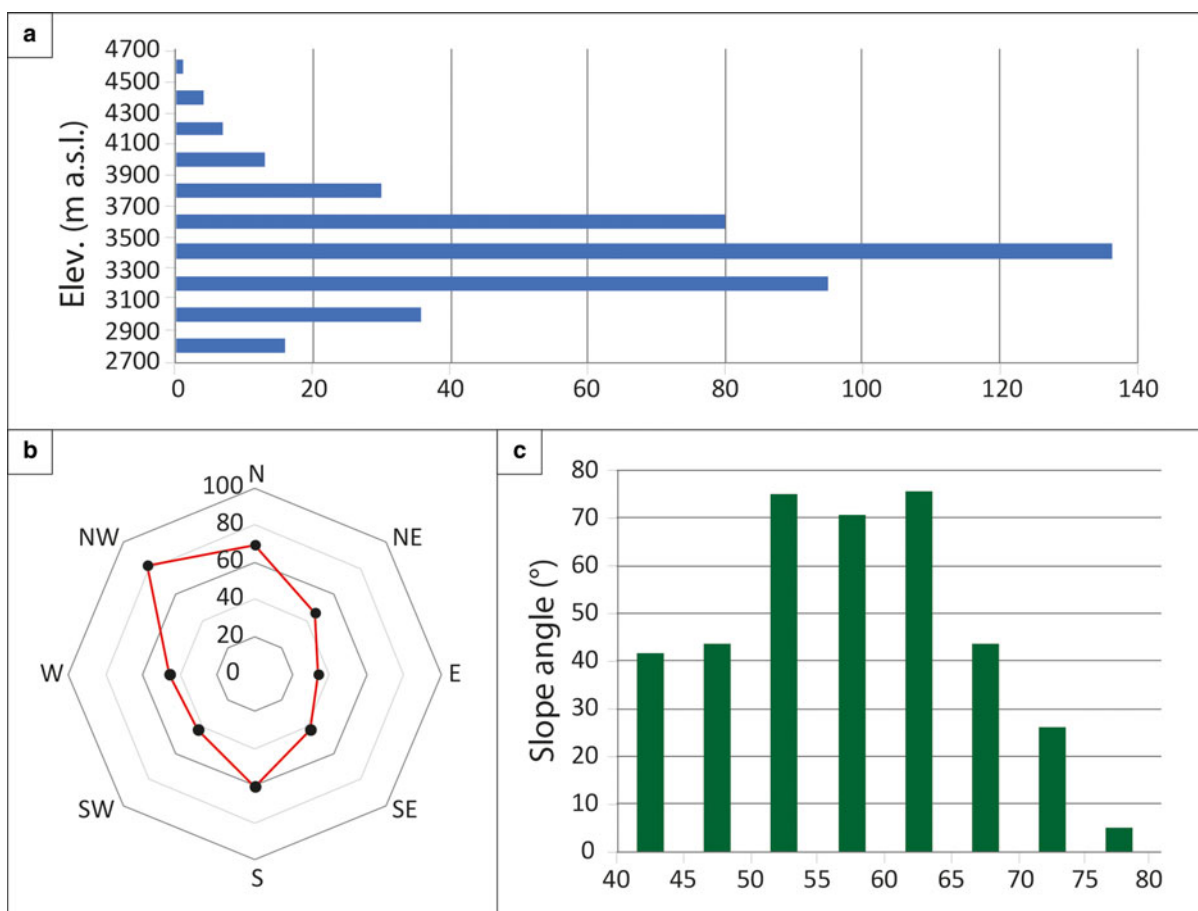

Fig. 4. Topographical characteristics of IAs in the MBM (Kaushik and others, 2021, modified): (a) elevation; (b) aspect and (c) slope angle; values correspond to the number of IAs. The analysis was performed using ASTER global DEM available at 25 m resolution.

existed since the mid-1970s, like the *World Glacier Inventory* (WGMS, 1989) or the *Randolph Glacier Inventory* (RGI), no data were available for IAs partly because IAs are not glaciers and therefore not systematically contained in these inventories. First steps have been made in the MBM by Guillet and Ravanel (2020) and Suvrat and others (2022b) while thickness losses also become significant as indicated by first observations and measurements, affecting the stability of recently deglaciated and permafrost-affected rock walls. The interactions between IAs and permafrost need to be better understood.

4.1. Variations in ice apron surface area since the 19th century

Using oblique historical imagery and a specifically developed photogrammetric inverse perspective method for extracting physical landscape measurements (see Guillet and others, 2020), Guillet and Ravanel (2020) documented the variations in surface area for six IAs from four north-oriented steep rock walls within the MBM since the termination of the LIA (see Fig. 3): one at Triangle du Tacul (3970 m a.s.l.) between 3570 and 3690 m a.s.l. (0.004 km^2 in 2018; slope angle: ~59°); two at Tour Ronde (3792 m), 3343–3594 m and 3600–3750 m (0.011 km^2 in 2018 and 0.005 km^2 in 2012, respectively; both ~55°); two at Grandes Jorasses (4208 m), 3220–3650 m and 3500–4000 m (0.016 km^2 in 2016 and 0.028 km^2 in 2017, respectively; both ~63°) and one at Aiguille des Grands Charmoz (3445 m), 2907–3185 m (in 2015; 0.0105 km^2 in 2012; ~52°).

Shrinkage is documented over all the considered IAs from the end of 1850s to the mid-to-late-1960s (Fig. 5). This period of shrinkage is followed by a short period of IA steadiness or expansion, from the early 1970s to the early 1990s. The Triangle du Tacul IA, for example, gained 11% of surface area between 1966 and 1988. This is certainly due to the significant precipitation and cooler temperatures than today (Auer and others, 2007) which allowed alpine glaciers to gain volume (see e.g. Vincent, 2002). Since the beginning of the 21st century, the study confirms the observations of the mountaineers, namely an accelerated shrinkage over all the six IAs. The shrinkage recorded since the termination of the LIA strongly varies between the different IAs. The upper IA of Grandes Jorasses experienced the lowest shrinkage, ~20% of the post-LIA surface area (−7400 ± 200 m^2), while other IAs show higher relative losses: 35% for Triangle du Tacul (−1940 ± 158 m^2), 40% for the upper IA of Tour Ronde (−3500 ± 147 m^2), 50% for the lower one (−1100 ± 127 m^2) and 60% for the lower IA of Grandes Jorasses (−28 440 ± 550 m^2) (Fig. 5). The most dramatic shrinkage affected the IA of Grands Charmoz, which melted completely during the summer of 2017 (Guillet and Ravanel, 2020).

Using very high-resolution optical images, Kaushik and others (2021) have quantified the surface area of the IAs in the MBM for 2012 (Pleiades 1B PAN and ortho-images IGN – *Institut national de l'information géographique et forestière*) and 2019 (Pleiades 1B PAN and Sentinel-2). Although manual mapping procedures are time-consuming, they enabled to map outlines of surface ice with the highest precision, an operation which remains difficult with automatic mapping, especially for very small snow/ice features (e.g. Paul and others, 2013). The work has recently been completed by Kaushik and others (2022b) by including the years
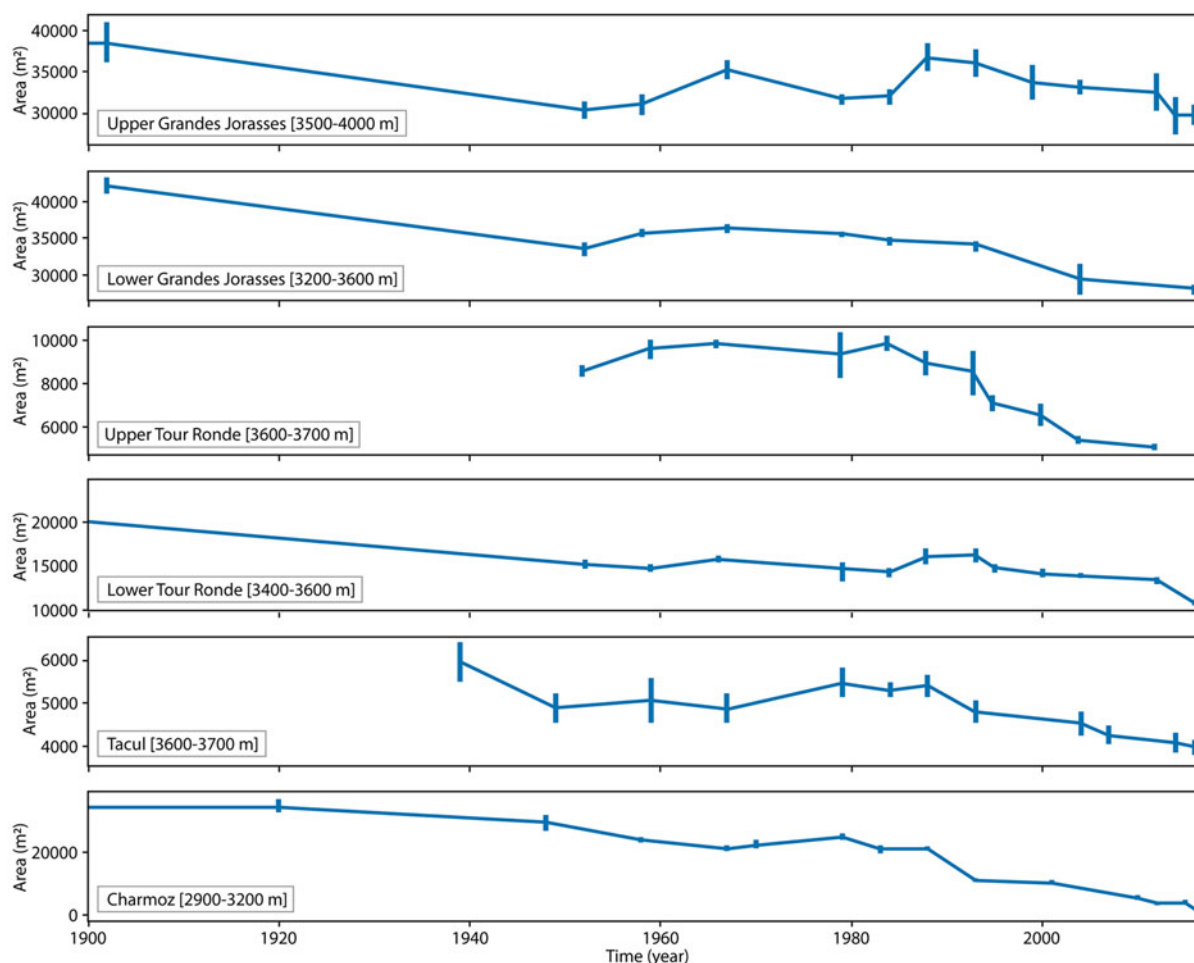

Fig. 5. Variations of surface area of six IAs in the MBM since the termination of the LIA (Guillet and Ravanel, 2020). Error bars represent the 95% confidence interval. Elevations are in m a.s.l.

1952 and 2001 from ortho-images IGN. The total surface area of IAs in 1952 was 7.93 km² and then dropped to 5.91 km² in 2001, 4.92 km² in 2012 and 4.21 km² in 2019 (Fig. 6). From 1952 to 2019, IAs have lost ~47% of their surface area, corresponding to an average rate of surface area loss of 0.78 km² decade⁻¹. The area loss was 25.4% from 1952 to 2001 compared to 30.6% from 2001 to 2019 (Fig. 6).

4.2. Significant recent changes in ice apron thickness

IAs are small ice masses located in mainly concave topographies (Kaushik and others, 2022b). The loss of surface is therefore related to the loss of thickness.

Mountaineers have widely experienced this loss through: (1) the disappearance of ice in many climbing routes (Mourey and others, 2019) or even on an entire rock wall, as in the cases of the north face of Aiguille des Grands Charmoz in 2017 (see Section 4.1) or the famous niche in the north face of Les Drus (3754 m a.s.l.) of which only a curved rest of ice remained in the most shaded area at the end of the recent hot summers of 2019 and 2022; (2) the emergence of spurs and boulders within IAs that were recently still continuous (e.g. at Triangle du Tacul where a spur appeared in 2003–04 in the centre of the lower IA and where new rocks now appear almost every year; see black dashes in Fig. 8); (3) the disconnection between current IA surfaces and mountaineering equipment used until the very beginning of the 2000s (Mourey and others, 2020). In the Gabarrou-Marquis route at Triangle du Tacul for example, ~6.2 m of ice had melted in 2020 since the early 2000s when a belay, now inaccessible, was still used on the right rim of the IA (Fig. 7a).

Such ice loss can also be revealed locally when topographic maps are updated. Since 2012, the IGN 3630OT Chamonix map 1: 25 000 (IGN, 2017) contains a new brownish tint corresponding to 'glacier retreat between 1980 and 2009' derived from aerial images of 2008 (Fig. 7b). Although not usable for our study given the steepness of the slopes, the new colours suggest the loss of IA area and thickness, confirmed by the comparison of aerial photos (Fig. 7b).

To quantify the IA-wide thickness loss and its spatial variability, we determined the annual mass balance for 2017 using stakes in the lower Triangle du Tacul IA (Fig. 8; aspect: 355° N, surface area: 0.04 km²; slope angle: 59°). Ten 2 m-long fibreglass stakes (1 m in the ice to measure the probable melt and 1 m outside to measure the possible accumulation) were installed on 29 March 2017. They were checked on 25 September 2017 and 16 March 2018. The hot summer of 2017 consistently melted 42–48 cm of ice over the whole IA (excluding the area covered by snow in

March 2017 and areas where snow avalanches and boulder falls destroyed the stakes; Fig. 8), i.e. a mean melting of 0.4 ± 0.03 m w.e. No mass gain or loss was detected between September 2017 and March 2018. Thus, we measured over 1 year a significant summer loss and no accumulation. This monitoring and previous observations (Guillet and Ravanel, 2020) suggest that summer melting combined with the absence of accumulation has probably been a fairly general trend since the early 2000s. The efficiency of the summer melting is corroborated by Kaushik and others (2022c) who investigated the evolution of the physical backscatter properties and surface changes of IAs by exploiting time series of X- and C-band synthetic aperture radar (SAR) images from PAZ and Sentinel-1 satellites. SAR data indeed provide information about the seasonal behaviour of IAs since physical changes of IA surfaces modify the backscattering of radar waves. The analysis of the temporal variations of the backscatter coefficient illustrates the effects of summer air temperatures on the surface of the IAs with a strong decrease in coefficient values indicating an increase in the liquid water content and thus the melting. Accumulation on IAs is severely hindered by surface topography, as only snowfall occurring within the 0 to −5°C temperature range can accumulate on slopes steeper than 30° (Guillet and Ravanel, 2020; Eidevåg and others, 2022). With the growing number of summer (Beniston and others, 2004; Zampieri and others, 2016) and winter (Beniston, 2005; Colucci and others, 2017) heat waves, such conditions have become rarer while smooth ice surfaces are not conducive to snow deposition under windy conditions. IAs are thus becoming particularly distinguishable (grey ice) in the MBM from other types of less steep and still snow-covered ice masses (see Fig. 1). The evolution of the colour of the IAs and their very high retreat rates over recent period contribute greatly to the darkening of the high-mountain slopes and give rise to fears of numerous disappearances in the near future.

4.3. Short-term effects on rock slope stability

Rockfalls >100 m³ have been surveyed in the MBM since 2007 (Ravanel and Deline, 2013; Ravanel and others, 2017a). Over the recent years, many small events have occurred in recently deglaciated areas due to retreat of IAs: following 2015, 2017, 2018, 2019, 2020 and 2022 summer heat waves, rockfall deposits have heavily accumulated at the foot of ice-covered rock walls (Fig. 9). Besides boulders formerly embedded into the ice and released as the ice melts, a high rockfall frequency from the margins of the shrinking IAs is observed. Ice vanishing often exposes perennially frozen and heavily fractured rock that the disappearance of the ice in the form of a cover or joints no longer allows to
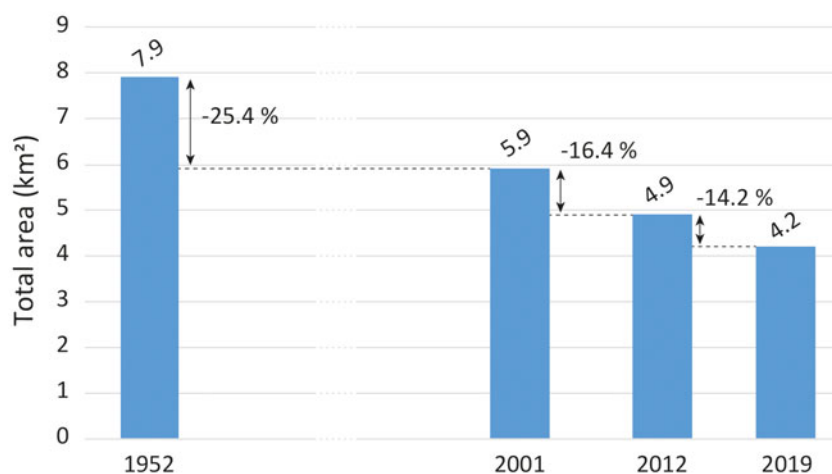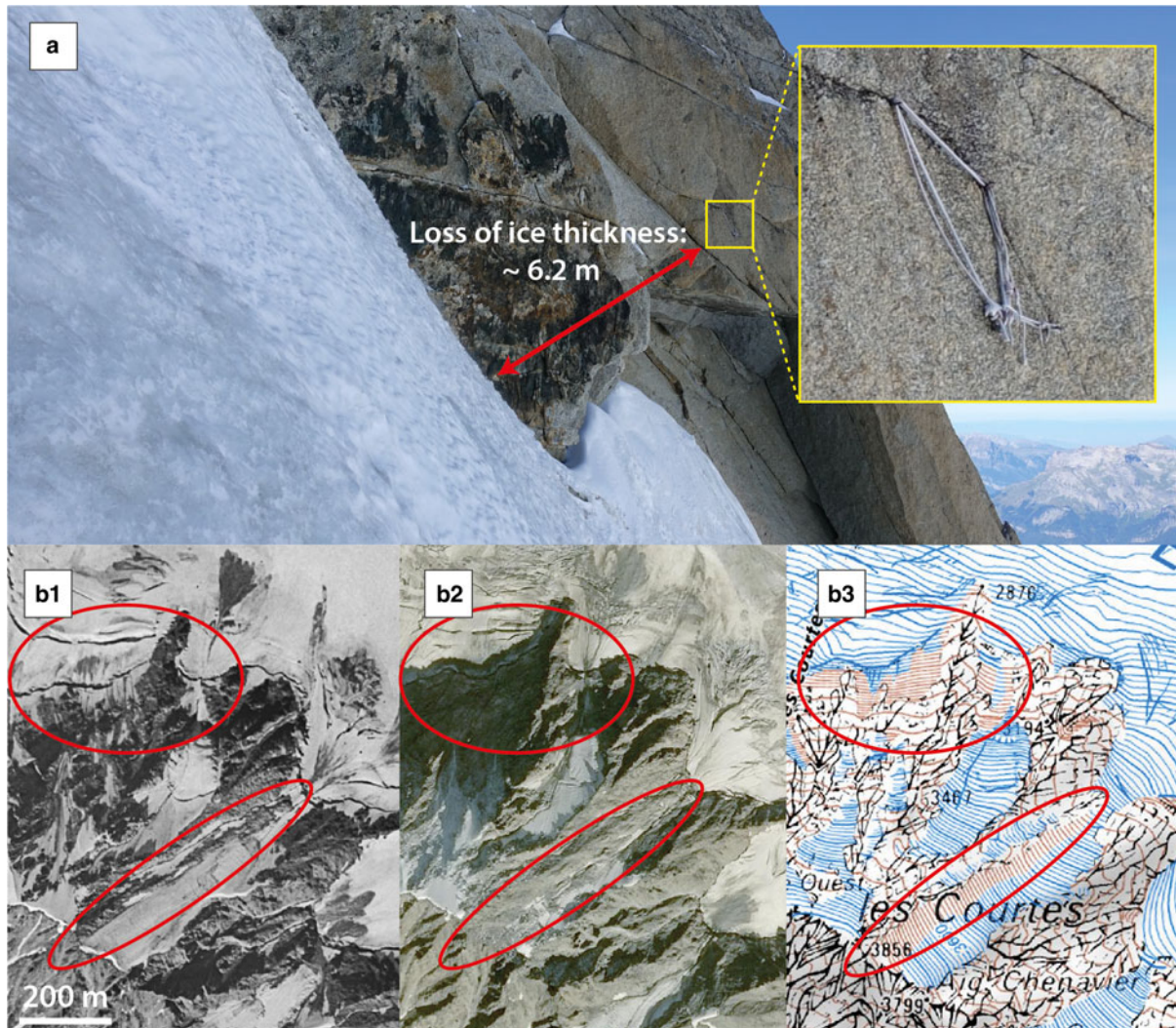

**Fig. 6.** Evolution of the total surface areas of IAs in the MBM over seven decades.

Fig. 7. Two examples of the thickness loss of IAs. (a) Loss of ~6.2 m of ice thickness at the Triangle du Tacul between the beginning of the 2000s, when permanent mountaineering equipment could be reached from the surface of the ice, and 2020. (b1) Left sidewall of the Argentière Glacier in 1952 (IGN orthophoto); (b2) in 2019 (Spot7 image); (b3) part of the IGN topographic map 3630OT Chamonix 1:25 000 that indicates (brown contours) the shrinkage of several IAs.

maintain on the slope (Davies and others, 2001; Krautblatter and others, 2013; Mamot and others, 2018; Kenner and others, 2022). At the scale of larger alpine faces like Monte Rosa east face (4634 m a.s.l., Italian Alps), Fischer and others (2011) showed that the sequence of the largest slope failures occurring during the last few decades is spatially connected to disappearing surface ice and further demonstrated the coupling between permafrost-related instability and the condition of adjacent ice masses. The case of the north face of Tour Ronde in 2020 sheds light on this point. An automatic camera was used to monitor the evolution of the face throughout the summer season (Fig. 10). Totally snow covered at the beginning of the summer, the IA underwent notable melting in July and a first rockfall occurred from a recently deglaciated area on 31 July. A second event occurred on 4 August, from an area directly upstream which had still been covered by ice a decade earlier. Later, a third rockfall occurred on 27 August just upstream of the previous one, in an area also covered by ice several decades ago. The two last events exposed massive ice in their scar (Fig. 10), confirming a permafrost context (Cremonese and others, 2011). This ice suggests a rockfall related to permafrost degradation (e.g. Gruber and Haeberli, 2007; Ravanel and others, 2017a). A rockfall of ~12 000 m³ (estimation from measurements on a 3-D model acquired by terrestrial LiDAR) finally took place on 13 August 2022 after three long

heat waves in the western European Alps (the summer of 2022 was the hottest ever recorded in France and in Chamonix – data *Météo France*) causing a probably unprecedented IA melting and a very significant heat input for the permafrost. While the melting of IAs likely destabilizes rock volumes almost immediately, the retreat of IAs also implies the development of a new direct air/rock connection in deglaciated areas – for the very first time in several millennia (see Section 6.2) –, generating permafrost degradation (active layer development, i.e. the formation of a sub-surface layer that thaws each year, and a deep and long-term warming from the surface), then triggering rockfalls (see also Haeberli and Gruber, 2009; Hartmeyer and others, 2020). The subsurface response of permafrost can be all the faster as the ice gives heat to the surrounding rock while melting (Hasler and others, 2011). IAs are thus first-order protective layers for permafrost (see e.g. Wegmann and others, 1998) since the thermal conductivity of the rock is much better than that of the ice and a thermal inertia arises from latent heat (Noetzli and others, 2007; Harris and others, 2009; Hasler and others, 2011). Heat therefore does not penetrate the ice well. Thus, the temperature variability at ~8 m depth (see Section 5) is much lower under the ice of the Tour Ronde IA than in the rock at the Aiguille du Midi (Magnin and others, 2015b) with a rather similar orientation and altitude.
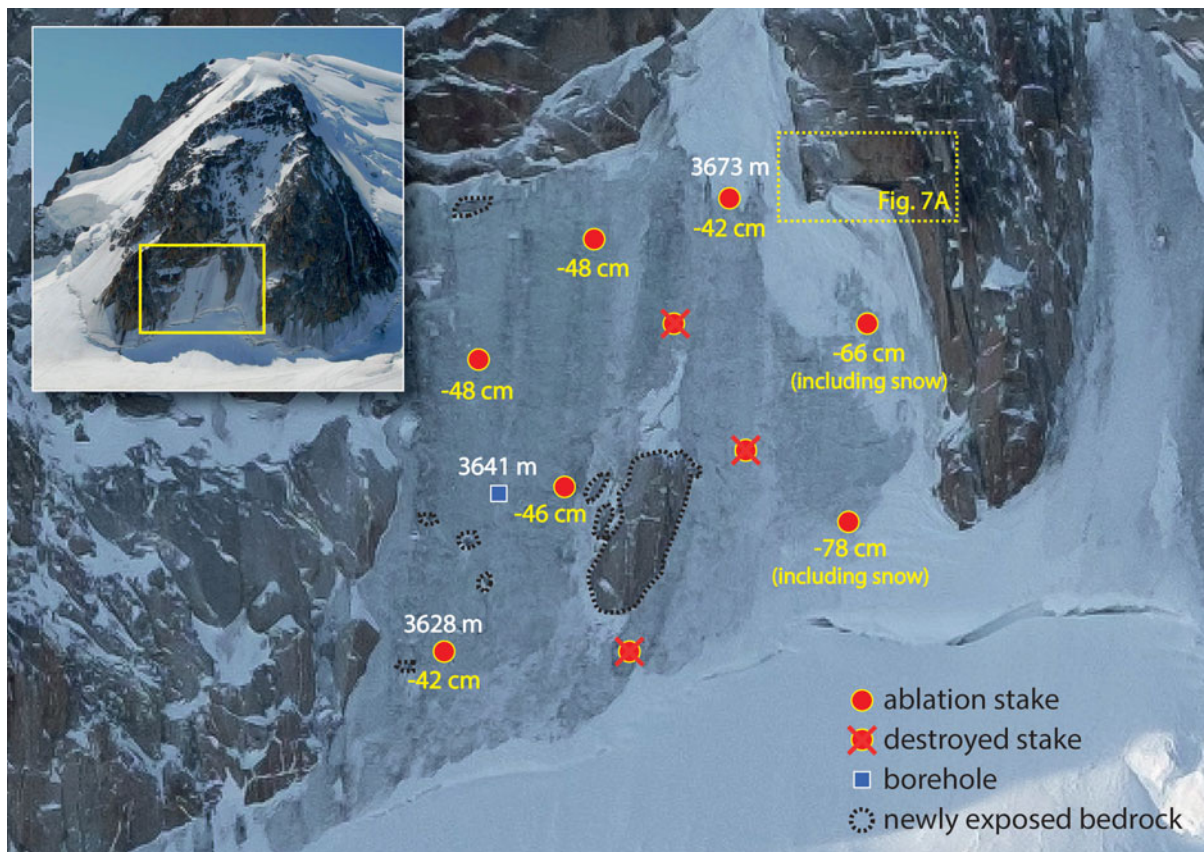
Fig. 8. Effects of a hot summer on the evolution of IAs: the example of the summer 2017 thickness loss in Triangle du Tacul. Elevation in m a.s.l. Outside areas covered with snow in early summer, mass balance was −0.4 ± 0.03 m w.e (only ablation occurred during the year).

5. Ice aprons: cold ice bodies

Given the spatial distribution of alpine permafrost (Boeckli and others, 2012; Magnin and others, 2015a) and cold-based glaciers (Suter and Hoelzle, 2002; Haeberli and others, 2004) which are frozen to bedrock (Waller, 2001; Faillettaz and others, 2011), IAs are interpreted as permafrost evidence (Haeberli and others, 1997; Gruber and Haeberli, 2007), and it has been assumed that IAs are composed of cold ice (Haeberli, 1975; Guillet and others, 2021). This thermal state had to be confirmed through recent systematic in situ temperature measurements in boreholes.

5.1. First two boreholes drilled in ice aprons

In high mountains, temperature measurements in boreholes have been used routinely to study the thermal regime of glaciers (Fisher, 1955; Haeberli and others, 1988, 2004; Haeberli and Funk, 1991; Lüthi and Funk, 2001; Suter and others, 2001; Suter and Hoelzle, 2002; MacDonell and others, 2013), rock glaciers (Arenson and others, 2002; Haeberli and others, 2006; PERMOS, 2019) and rock wall permafrost (Harris and others, 2009; Magnin and others, 2015b; Pogliotti and others, 2015). In the MBM, recent ice temperatures (Vincent and others, 2007a, 2007b) have been compared with older data (Lliboutry and others, 1976; Vincent and others, 2020), while measurements have been carried out at the Tête Rousse and Taconnaz Glaciers because of risks for the valleys (Gilbert and others, 2012, 2015). In order to better understand the thermal regime of IAs and its relationships with the underlying permafrost, two boreholes in IAs were drilled to bedrock and equipped (Figs 11a, b) with a *Geoprecision* thermistor chain (Dallas DS18S20, accuracy: ±0.25° C, resolution: 0.065°C): on the north face of Tour Ronde (nine sensors up to 880 cm deep, installed in December 2016), and at

Triangle du Tacul (four sensors up to 100 cm deep, installed in March 2017) (Ravanel and others, 2017b). These chains were installed in high-resistance polyurethane (PU) tubes cased in October 2016 in boreholes drilled normal to the ice surface using a portable steam-driven ice drill (Heucke, 2003). Foam pads were inserted between the sensors to prevent heat advection by air. Temperature was recorded every 4 h by a *Geoprecision* logger (Dallas M-Log5W). Setting up required significant mountaineering skills, but maintenance was even more challenging. At Triangle du Tacul, the summer 2017 heat wave melted almost half of the thickness of the IA (see Section 4.2) at the borehole location, exposing three sensors to free air. At Tour Ronde, the early heat wave of summer 2017 produced rockfalls from the upper margin of the IA that strongly damaged the upper part of the borehole. The following winter, an avalanche destroyed the logger.

5.2. Cold ice stuck to the permafrost

At Tour Ronde, we acquired a bit more than 10 months of data (2 December 2016–11 October 2017; Fig. 11c). Near-surface IA temperature is heavily correlated with air temperature, while only seasonal air temperature signal affects ice temperature below 5 m depth. The lowest temperature at 5 m depth is recorded in the early summer (Fig. 11e). From 2 December 2016 to 30 May 2017, sensors at −10, −30 and −50 cm displayed very high variability, with two periods (21 March–13 April; 25 April–24 May) of similar temperatures with reduced variability that suggests the setting of a snow cover (see e.g. Magnin and others, 2017), confirmed by photos automatically taken from the nearby Aiguille du Midi cable-car station. Influx of warm air affects the MBM from the second 10 d period of May, evidenced by the
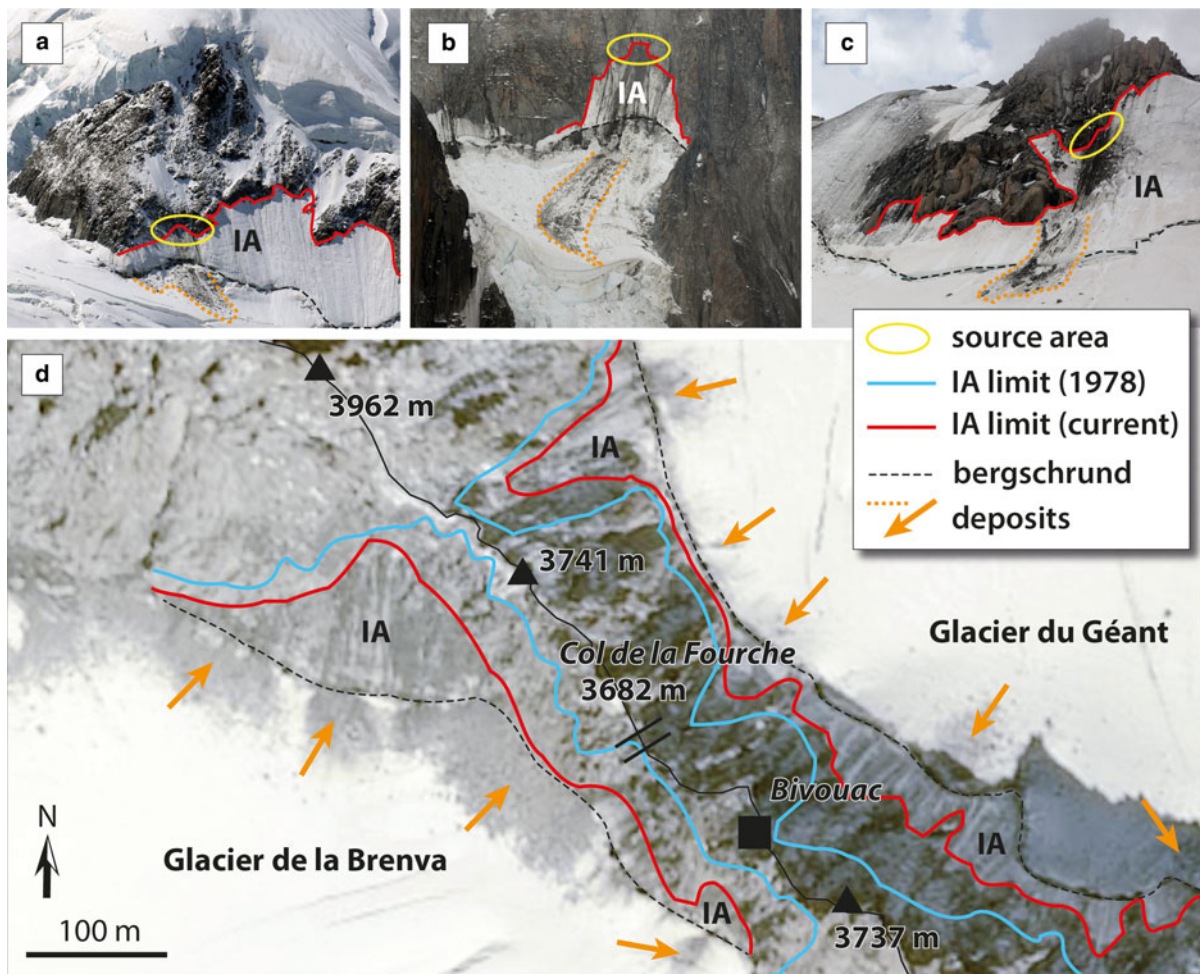
Fig. 9. Rockfall deposits at the foot of: (a) the north face of Rocher du Petit Plateau (3680 m a.s.l.; photo 13 August 2019); (b) the north side of Col du Diable (3770 m; photo 8 August 2018); (c) the north face of Pointe Lachenal (3565 m; photo 13 August 2019) and (d) along the Brenva ridge on the French–Italian border (SPOT6 image, late summer 2018). Areas between the upper limits of the IAs in 1978 (blue) and 2018 (red) are the main source of the rockfalls.

largely positive temperature measured by the 10 cm-deep sensor in the rock on the left margin of the IA, at the borehole altitude. The available heat melted the snow, generating a loss of insulation (see e.g. Magnin and others, 2017), and warmed the exposed ice. This surface change lowered the surface albedo during the time of maximum incoming solar radiation, which at this IA with its exposure of azimuth N12° is especially important during hours of the morning sun. Following 30 May, the three shallowest sensors recorded significant warming of the ice, with temperatures close to the melting point. Between 7 and 12 June, these temperatures became positive as the sensors were exposed to free air. This significant melting was favoured by high air temperature and still the exposure of the IA to direct sunlight. On 15 June, the ice at the level of the sensor −100 cm reached temperature close to the melting point. The sensor seems exposed to free air on 7 July, suggesting a melting of ∼1 m of ice between 7 June and 7 July. Initially positioned at −150 cm, the fifth sensor indicated a temperature of 0°C from 8 July but remained buried in the ice (no positive temperature recorded).

The lowest mean temperature (−6.6°C) for the available period was found for the sensor initially located at −250 cm. At the ice–rock interface, the mean 10 month temperature was −4.8°C, confirming the presence of cold permafrost in the rock slope. At this depth (originally −880 cm), the lowest temperature is recorded on 13 June (−6.0°C) while the peak temperature was not yet reached on 11 October 2017 (−4.2°C), when the equipment was damaged. On 2 December 2016, this temperature was −4.4°C, before decreasing: maximum temperature at the base of the IA is

therefore likely attained in November. At this depth, a jump in the temperature curve is recorded several days from 12 June 2017 (Fig. 11e), related to a rockfall detected with the Aiguille du Midi camera. It is conceivable that the rockfall damaged the PU tube, allowing liquid water to flow down to the bottom of the borehole, thus temporarily modifying the temperature.

At Triangle du Tacul, temperature was continuously recorded between 1 April 2017 and 31 March 2018 (Fig. 11d). Because of the IA thinness, ice temperature is extremely dependent on air temperature. The sensor at −10 cm recorded significant ice warming from 3 May, leading to its free air exposure on 16 May. The sensor initially at −30 cm indicated ice temperature close to the melting point around 28 May, and was exposed on 12 June. The −50 cm sensor indicated a temperature of 0°C from 12 June, and positive temperature from 16 July, as the mass balance (cf. Section 4.2) indicates a loss of thickness of 46–48 cm near the borehole (Fig. 8). In view of the strong documented ice losses (see Fig. 11f), only the mean annual temperature at the rock–ice interface can be considered: −8.1°C. The annual temperature range is very significant there due to the very thin ice: 0°C on 6 August 2017 (ice temperature almost reaches the melting point during two short periods: 3–5 August and 26 August–3 September), and −20.2°C on 20 February 2018.

These recordings confirm that – outside warm periods during which ice temperature close to the surface can reach 0°C eventually before melting – the IAs are cold ice settled on terrain with negative subsurface temperatures, i.e. stuck to the permafrost-affected bedrock. They are part of the permafrost-related periglacial
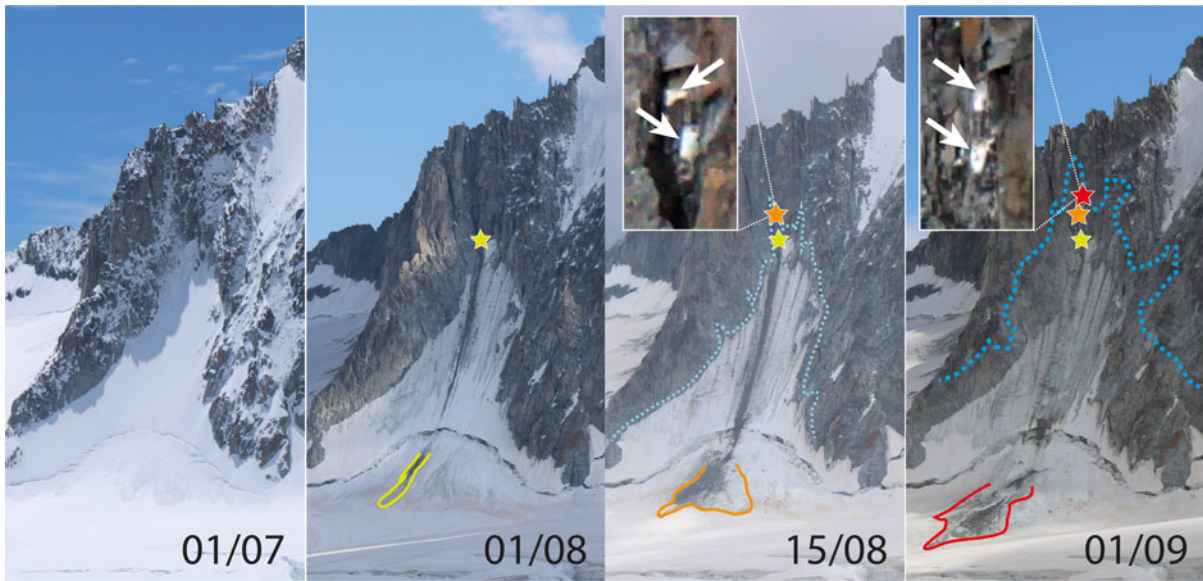
Fig. 10. Evolution of the north face of Tour Ronde during the summer 2020 and in 2022. The lower IA, covered with snow at the beginning of the summer 2020 is almost snow-free at the end. Three rockfalls occurred from the upper limit of the IA: on 31 July and on 4 and 27 August (stars: sources). The last two exposed massive ice (arrows) in their scar. Light blue and blue dashed lines: IA limits in 2009 and the 1880s, respectively. A much larger rockfall finally occurred on 13 August 2022.

environment. The basal sliding processes are therefore largely excluded as a consequence of cold-bed conditions, explaining the stability of ice on such steep slopes.

6. Ice aprons: quasi-static millennial ice

There was a fundamental lack of knowledge about the age and dynamics of the ice composing IAs. As the low thickness probably
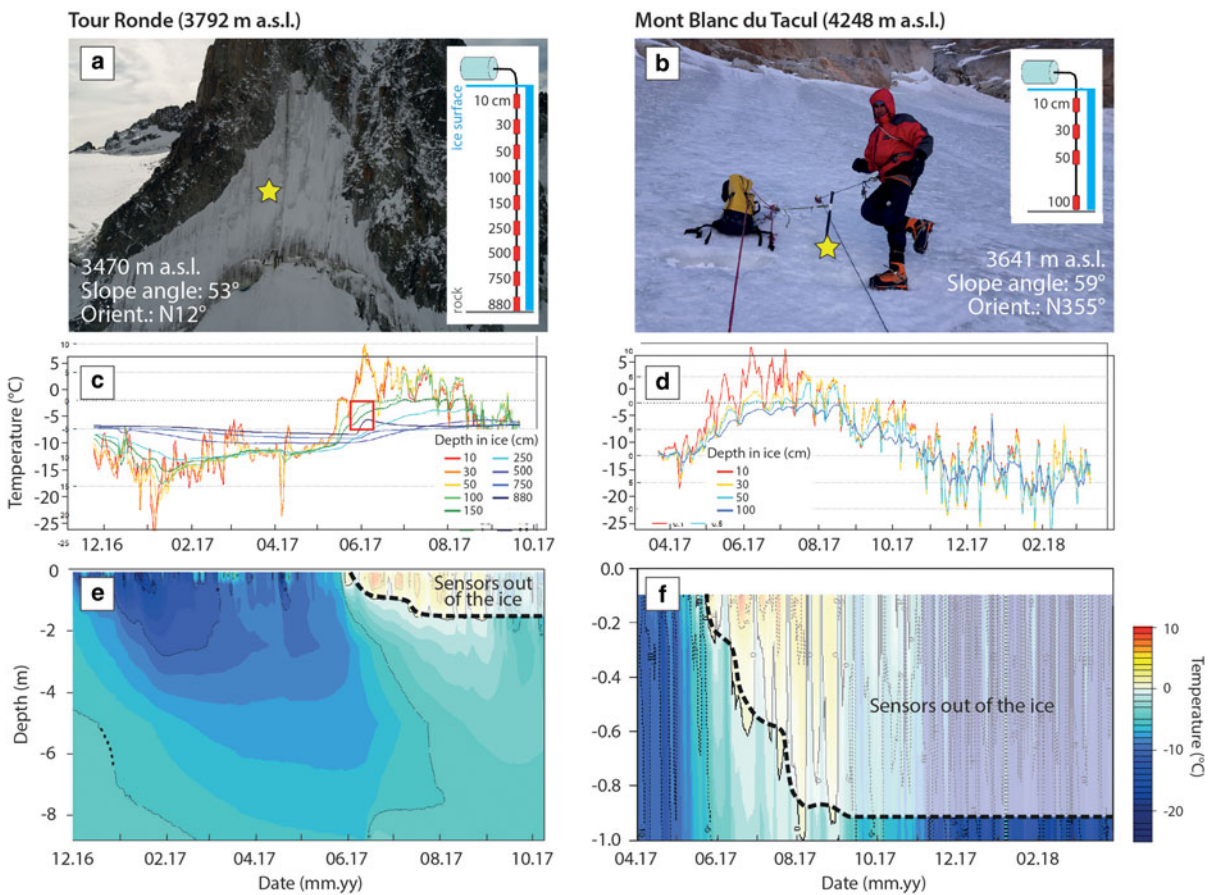
Fig. 11. Thermal regime of two IAs in the MBM. (a, b) borehole location and thermistor chain at Tour Ronde and Triangle du Tacul. (c, d) Tour Ronde and Triangle du Tacul daily temperatures at different depths; at Tour Ronde, the jump in temperature at 8.8 m depth in June 2017 (red box) is certainly linked to liquid water flowing to the bottom of the borehole, following its damage by a rockfall; at Triangle du Tacul, three of the four sensors came out of the ice due to its melting. (e, f) Tour Ronde and Triangle du Tacul modelled daily temperature from surface to 8.8 and 1.0 m deep, respectively.

prohibits any significant ice flow, it was believed that the analysis of IA ice structure would bring new insights into dynamics of IAs. Guillet and others (2021) addressed these points by studying ice cores sampled from Triangle du Tacul. Three 60 cm-long ice cores with a diameter of 5.5 cm were drilled to bedrock close to the borehole (see Fig. 8) in spring 2018 and 2019 using a portable drilling system (see Montagnat and others, 2010). One ice core was used to study likely lattice preferred orientation of ice crystals in order to highlight potential variations in ice structure with depth. The two remaining ice cores were used for age-dating, also by Guillet and others (2021).

6.1. Simple shear as the main regime for the deformation of ice-apron ice

To observe lattice preferred orientation, as well as grain shape and size, thin sections were sampled in one of the ice cores, using standard protocols for thin section preparation (see e.g. Schwarz and others, 1981; Durand and others, 2006). Thin sections were typically 4–5 cm wide and 0.4–0.5 cm thick. Guillet and others (2021) used an Automatic Ice-Texture Analyser (Wilson and others, 2003) to measure lattice preferred orientation.

Results from Guillet and others (2021) are presented on pole diagrams in stereographic projections in Figure 12 and quantify the statistical distribution of c-axis orientations (the optical birefringence axis, normal to the basal plane of the ice crystallographic structure; see: Alley and others, 1995). Guillet and others (2021) described c-axis distributions clustered around a single vertical maximum with most grains in the analysed samples oriented parallel to the core axis (reddish colours in Fig. 12). Several tilted grains (greenish colours in Fig. 12) could be observed within the ice core. Guillet and others (2021) further reported a sharp transition in ice lattice preferred orientation at 5 cm above bedrock, with an increase in the concentration of tilted grains, which they interpreted as resulting from the increase in the concentration of impurities in the ice, preventing effective recrystallization. This phenomenon has been widely observed and described in the scientific literature (see e.g. Thorsteinsson and others, 1996; Weiss and others, 2002). Statistical distributions of c-axis orientations in ice have been vastly documented and strong lattice preferred orientation are often attributed to the deformation of ice under simple shear and dynamic recrystallization under glacier conditions (see e.g. Hudleston, 1977; Hudleston, 2015). As the ice is deformed in simple shear, the single maximum distribution of c-axis orientations is typically oriented normal to the shear plane. This is reinforced by recrystallization (Journaux and others, 2019). According to Guillet and others (2021), the single maximum pattern observed in Triangle du Tacul ice likely results from a quasi-stationary shear regime, with a plane parallel to the surface slope of the IA.

6.2. Ice aprons as a glacial heritage

The above considerations and the significant melt of IAs during the recent decades suggest the outcropping ice to be of millennial age. Considering previous work focusing on the age of alpine glaciers (see e.g. Jenk and others, 2009; Gabrielli and others, 2016; Uglietti and others, 2016; Zipf and others, 2016; Feng and others, 2019; Preunkert and others, 2019a, 2019b; Bohleber and others, 2020), Guillet and others (2021) expected the age of near-bedrock ice in IAs to be ranging between several hundred and several thousand years. A dating method specific to ice containing no vegetal leftover and suitable for potential ice ages older than a few hundred years was therefore considered. The authors specifically used ^{14}C in particulate organic carbon (POC) associated with a recent sample preparation method successfully applied to near-bedrock ice from cold-based glaciers at high altitude (Hoffmann and others, 2018; Preunkert and others, 2019a) and lower altitude (Bohleber and others, 2018). They focused on the lower part of the ice cores to avoid potential near-surface age-biasing artefacts, did however omit the lowest few centimetres of the cores to avoid macroscopic impurities – in greater concentration near bedrock (Guillet and others, 2021). Sample preparation (ice decontamination, melting, filtering and combustion) is described by Preunkert and others (2019a). POC average concentration of the samples was 330 ± 140 ng C g^{-1} (Guillet and others, 2021), i.e. 15 times higher than values found in the lowest metres of the neighbouring Col du Dôme Glacier (Preunkert and others, 2019b), located at 4250 m a.s.l. and 5 km southwest of Triangle du Tacul. This difference was interpreted as resulting from the altitude difference and the presence of biogenic material near the IA during its formation (Guillet and others, 2021). Radiocarbon analyses were performed at the mass spectrometer accelerator at the Curt-Engelhorn Centre Archaeometry (Manheim, Germany). Three ages were obtained: (1) a mean calibrated ^{14}C-age of 2640 ± 130 year cal BP on the 2018 core between 32 and 52 cm depth, averaging the ice age over 20 cm (Guillet and others, 2021), corresponding to Göschener I, a 3000–2300 year BP alpine cold period (Zoller and others, 1966; Boxleitner and others, 2019); (2) 630 ± 55 year cal BP between 30 and 40 cm depth and 2840 ± 175 year cal BP between 40 and 49 cm on the 2019 core (Guillet and others, 2021). Therefore, the mean 2019 sample age is 1735 year cal BP (with a mean high time gradient of 220 years cm^{-1}), i.e. 950 years younger than the 2018 sample. This difference was explained by the authors as resulting from an imperfect overlap of the covered time periods within the two sampling depths of the two cores due to (1) an inhomogeneous spatial accumulation distribution at this IA, affecting the age–depth model, (2) variability of isochronology distance to bedrock due to sub-glacial topography and (3) spatial variability of the ice melt (ablation). Using the age–depth calculation from the 2019 ice core, Guillet and others (2021) further suggest an age of ~5500 year BP as a first crude estimate of the very near bedrock ice at Triangle du Tacul.

This age is consistent with other ages of basal ice in high-altitude cold-based alpine glaciers: 7000 year cal BP at Alto dell'Ortles (3905 m a.s.l., central alps, Italy) (Gabrielli and others, 2016), 5600 year cal BP at Col du Dôme (Preunkert and others, 2019b) and 5000 year cal BP at Chli Titlis (3030 m a.s.l, central alps, Switzerland) (Bohleber and others, 2018) while older ages exist as >15 000 cal BP at Colle Gnifetti (4455 m a.s.l., Monte Rosa, Switzerland) (Jenk and others, 2009; Hoffmann and others, 2018; see also: Gäggeler and others, 1983; Lüthi and Funk, 2000). Unlike the aforementioned glaciers, where basal ice is located tens of metres below the surface, IAs possibly offer a quick access with appropriate mountaineering skills to thousands of years old ice.

In the coming years, to better appreciate the palaeo-environmental potential of IAs through the establishment of an age model and the detection of chemical tracers of air pollution sources, to model their effects on the underlying permafrost (new borehole temperature measurements and modelling) and to ensure continuous monitoring of thickness variations (LiDAR or glaciological mass balance) is imperative while, in the meantime, strengthening the effort towards the understanding of IA dynamics (rheology, accumulation/ablation and related local factors) in the alps and outside is needed.

7. Conclusions and perspectives

Almost 60 years after first observations in the European Alps, research on IAs has been carried out in the MBM since 2015 with different methodologies and instruments:
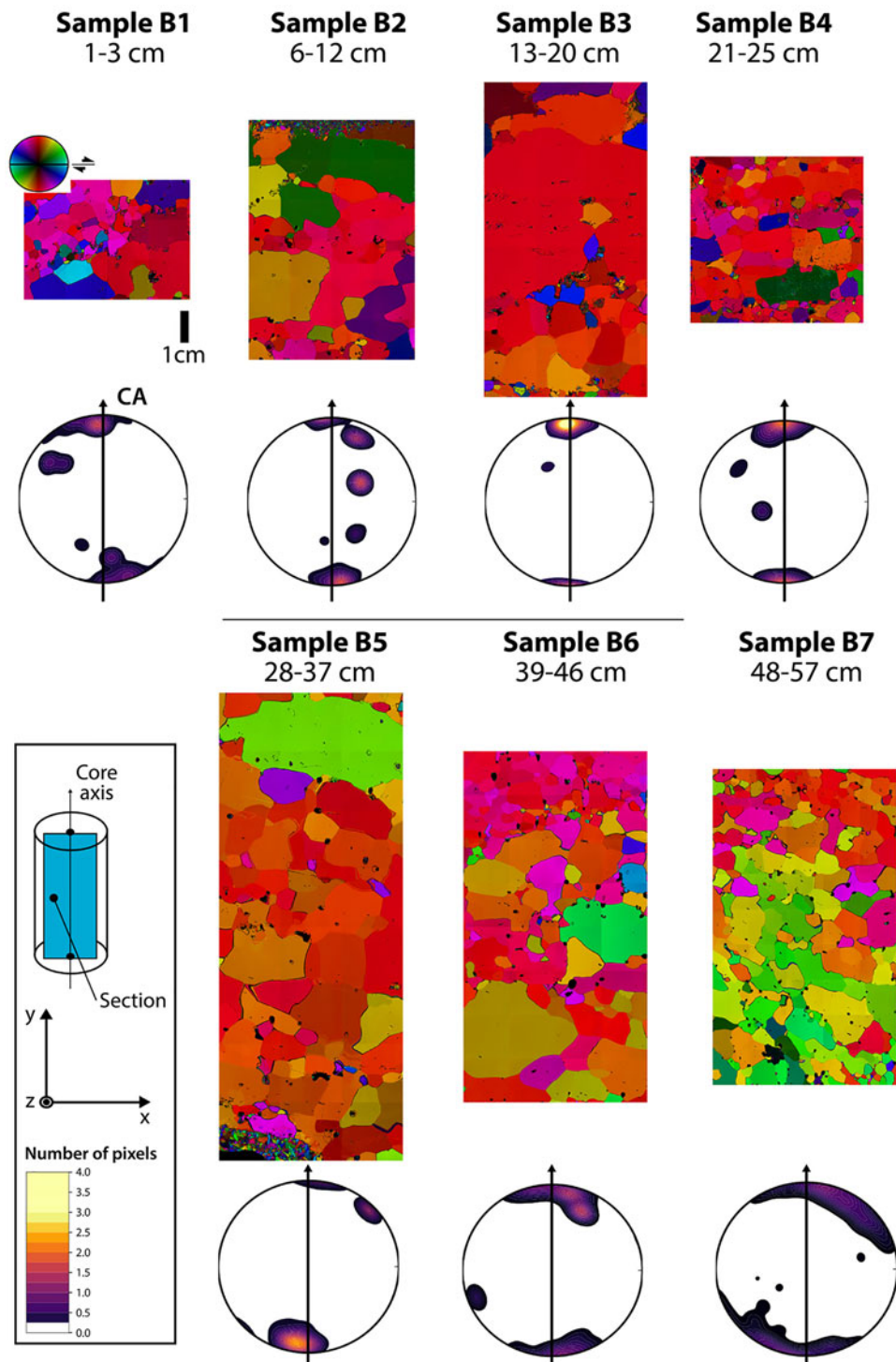
Fig. 12. *c*-Axis lattice preferred orientation pole figures and orientation colour-coded images displaying the *c*-axis orientations for all the thin sections of the Triangle du Tacul ice core (Guillet and others, 2021). Crossed out sections represent destroyed portions of the ice core. Note that depth representation is not to scale and depths have been rounded to the nearest value. In most pole figures, statistical distributions of *c*-axis orientations are clustered around a single maximum. Second maxima on section 2 is the consequence of the relative weight of the two greenish crystals in the statistical distribution of the sample. *c*-Axis orientations on the orientation colour-coded images are given by the colour scale on the top left. The colour code on the pole figures represents the density of *c*-axis orientations at the pixel scale (1 pixel = 20 μm).

- the main topographic characteristics of IAs have been studied *via* remote sensing;
- the surface of six IAs has been reconstructed since the termination of the LIA from aerial and terrestrial photographs while the surface of all the IAs of the massif was reconstructed from high-resolution aerial and satellite images for four dates between 1952, 2001, 2012 and 2019;
- 10 ablation stakes were used to calculate a first ever IA's mass balance;
- borehole equipped with temperature sensors were drilled in two IAs of different thicknesses (8.8 and 1.0 m) in order to measure the temperature of the ice and at the ice–rock interface;
- an automatic camera allowed us to observe the temporal and spatial relationship between the retreat of an IA and the stability of its rock environment during a summer season;
- three short ice cores were extracted from an IA to document the deformation and age of the ice.

Finally, to the definition 'very small (generally <0.1 km^2) [perennial] ice bodies of more or less irregular outline due to high-ruggedness topographies, lying on steep slopes' (an arbitrary slope threshold of 40° is commonly used to differentiate IAs from other stationary ice bodies such as permanent snow patches) with a quasi-stationary shear regime (very low ice creep), can be added that they are mainly located above the regional equilibrium line altitude (∼3000–3100 m a.s.l. in the MBM region) in permafrost context as illustrated by the mean annual temperatures of ∼−5 and −8°C measured at the base of two IAs. The small ice thickness, coupled with this cold context, indeed implies almost near-zero movement of the ice. IAs occupy a very small part of the ice-covered surfaces (4.2 km^2 in the MBM, i.e. 2.6% of its total ice surface area) and they are currently not or only slightly fed by snow, while they can lose several tens of centimetres of thickness during a single hot summer. This loss results in a very significant retreat, as shown by the dramatic 50% reduction of IA surface area in the MBM since the 1950s. This shrinkage leads to a darkening of mountain appearance, increasing difficulties for mountaineering and risks of rockfall. This also represents a threat of disappearance of these ice masses that are several hundred to several thousand years old.

The combination of the current IA high retreat rates, the reduction of their albedo accelerating melting, their reduced thicknesses and the acceleration of global warming leads concern with regard to a very large number of IAs disappearing in the short term. At the present rate (Kaushik and others, 2022*b*), the IAs in the MMB would lose another half of their surface area within 20 years. IAs thus seem to be among the most vulnerable components of the mountain cryosphere.

References

Alley R, Gow A and Meese D (1995) Mapping *c*-axis fabrics to study physical processes in ice. *Journal of Glaciology* **41**(137), 197–203. doi: 10.3189/S0022143000017895

Arenson L, Hoelzle M and Springman S (2002) Borehole deformation measurements and internal structure of some rock glaciers in Switzerland. *Permafrost and Periglacial Processes* **13**(2), 117–135. doi: 10.1002/ppp.414

Armstrong T, Roberts B and Swithinbank C (1973) *Illustrated Glossary of Snow and Ice.* Scott Polar Research Institute, Special Pub. No. 4, 2nd Edn.; Menston Yorkshire, UK: The Scholar Press Ltd., 60 p. doi: 10.3189/S0022143000020499

Auer I and 6 others and others (2007) HISTALP – historical instrumental climatological surface time series of the Greater Alpine region. International *Journal of Climatology* **27**(1), 17–46. doi: 10.1002/joc.1377

Beniston M (2004) The 2003 heat wave in Europe: a shape of things to come? An analysis based on Swiss climatological data and model simulations. *Geophysical Research Letter* **31**(2), L02202. doi: 10.1029/2003GL018857

Beniston M (2005) Warm winter spells in the Swiss Alps: strong heat waves in a cold season? A study focusing on climate observations at the Saentis high mountain site. *Geophysical Research Letters* **32**(1), L01812. doi: 10.1029/2004GL021478

Benn DI and Evans DJA (2010) *Glaciers and Glaciation*, 2nd Edn, London: Hodder Education, 802 p.

Berthier E and 7 others (2005) Surface motion of mountain glaciers derived from satellite optical imagery. *Remote Sensing of Environment* **95**(1), 14–28. doi: 10.1016/j.rse.2004.11.005

Berthier E and 10 others (2014) Glacier topography and elevation changes derived from Pléiades sub-meter stereo images. *The Cryosphere* **8**(6), 2275–2291. doi: 10.5194/tc-8-2275-2014

Berthier E, Cabot V, Vincent C and Six D (2016) Decadal region-wide and glacier-wide mass balances derived from multi-temporal ASTER satellite digital elevation models. Validation over the Mont-Blanc area. *Frontiers in Earth Science* **4**, 63. doi: 10.3389/feart.2016.00063

Bertini G, Marcucci M, Nevini R, Passerini P and Sguazzoni G (1985) Patterns of faulting in the Mont-Blanc granite. *Tectonophysics* **111**, 65–106. doi: 10.1016/0040-1951(85)90066-6

Bhutiyani MR (2011) Ice apron. In Singh VP, Singh P and Haritashya UK (eds). *Encyclopedia of Snow, ice and Glaciers*. Dordrecht: Springer Netherlands, pp. 581–582. doi: 10.1007/978-90-481-2642-2_254

Boeckli L, Brenning A, Gruber S and Noetzli J (2012) Permafrost distribution in the European Alps: calculation and evaluation of an index map and summary statistics. *The Cryosphere* **6**(4), 807–820. doi: 10.5194/tc-6-807-2012

Bohleber P, Hoffmann H, Kerch J, Sold L and Fischer A (2018) Investigating cold based summit glaciers through direct access to the glacier base: a case study constraining the maximum age of Chli Titlis glacier, Switzerland. *The Cryosphere* **12**(1), 401–412. doi: 10.5194/tc-12-401-2018

Bohleber P, Schwikowski M, Stocker-Waldhuber M, Fang L and Fischer A (2020) New glacier evidence for ice-free summits during the life of the Tyrolean Iceman. *Scientific Reports* **10**, 20513. doi: 10.1038/s41598-020-77518-9

Boxleitner M and 6 others (2019) The ^{10}Be deglaciation chronology of the Göschenertal, central Swiss Alps, and new insights into the Göschenen Cold Phases. *Boreas* **48**, 867–878. doi: 10.1111/bor.12394

Bussy F and von Raumer JF (1994) U–Pb geochronology of Palezoic magmatic events in the Mont-Blanc crystalline massif, Western Alps. *Swiss Bulletin of Mineralogy and Petrology* **74**, 514–515.

Cogley JG and 10 others (2011) *Glossary of glacier mass balance and related terms.* IHP-VII Technical Documents in Hydrology, 86 – IACS Contribution, UNESCO–International Hydrological Programme, Paris, 114 p.

Colucci RR, Giorgi F and Torma C (2017) Unprecedented heat wave in December 2015 and potential for winter glacier ablation in the eastern Alps. *Scientific Reports* **7**, 7090. doi: 10.1038/s41598-017-07415-1

Cremonese E and 5 others and others (2011) An inventory of permafrost evidence for the European Alps. *The Cryosphere* **5**, 651–657. doi: 10.5194/tc-5-651-2011

Davesne G, Fortier D and Domine F (2022) Properties and stratigraphy of polar ice patches in the Canadian High Arctic reveal their current resilience to warm summers. *Arctic Science* **8**(2), 414–449. doi: 10.1139/as-2021-0011

Davies MCR, Hamza O and Harris C (2001) The effect of rise in mean annual temperature on the stability of rock slopes containing ice-filled discontinuities. *Permafrost and Periglacial Processes* **12**(1), 137–144. doi: 10.1002/ppp.378

Dehecq A and 5 others (2016) Elevation changes inferred from TanDEM-X data over the Mont-Blanc area: impact of the X-band interferometric bias. *IEEE Journal of Selected Topics in Applied Earth Observations and Remote Sensing* **9**(8), 3870–3882. doi: 10.1109/JSTARS.2016.2581482

Dematteis N, Giordan D, Troilo F, Wrzesniak A and Godone D (2021) Ten-year monitoring of the Grandes Jorasses glaciers kinematics. Limits, potentialities, and possible applications of different monitoring systems. *Remote Sensing* **13**(15), 3005. doi: 10.3390/rs13153005

Durand G and 5 others (2006) Ice microstructure and fabric: an up-to-date approach for measuring textures. *Journal of Glaciology* **52**(179), 619–630. doi: 10.3189/172756506781828377

Durand Y and 5 others (2009) Reanalysis of 47 years of climate in the French Alps (1958–2005): climatology and trends for snow cover. *Journal of Applied Meteorology and Climatology* **48**(12), 2487–2512. https://doi.org/10.1175/2009JAMC1810.1.

Eidevåg T, Thomson ES, Kallin D, Casselgren J and Rasmuson A (2022) Angle of repose of snow: an experimental study on cohesive properties. *Cold Regions Science and Technology* **194**, 103470. doi: 10.1016/j.coldregions.2021.103470

Faillettaz J, Sornette D and Funk M (2011) Numerical modeling of a gravity-driven instability of a cold hanging glacier: reanalysis of the 1895 break-off of Altelsgletscher, Switzerland. *Journal of Glaciology* **57**(205), 817–831. doi: 10.3189/002214311798043852

Fallourd R and 5 others and others (2011) Monitoring temperate glacier displacement by multi-temporal TerraSAR-X images and continuous GPS

measurements. *IEEE Journal of Selected Topics in Applied Earth Observations and Remote Sensing* 4(2), 372–386. doi: 10.1109/JSTARS.2010.2096200

Feng Z and 7 others and others (2019) Dating glacier ice of the last millennium by quantum technology. *Proceedings of the National Academy of Sciences* 116(18), 8781–8786. doi: 10.1073/pnas.1816468116

Fischer L, Eisenbeiss H, Kääb A, Huggel C and Haeberli W (2011) Monitoring topographic changes in a periglacial high-mountain face using high-resolution DTMs, Monte Rosa East Face, Italian Alps. *Permafrost and Periglacial Processes* 22(2), 140–152. doi: 10.1002/ppp.717

Fisher JE (1955) Internal temperatures of a cold glacier and conclusions therefrom. *Journal of Glaciology* 2(18), 583–591. doi: 10.3189/002214355793702163

Flotron A (1977) Movement studies on a hanging glacier in relation with an ice avalanche. *Journal of Glaciology* 19(81), 671–672. doi: 10.3189/S0022143000029592

Gabrielli P and 5 others and others (2016) Age of the Mt. Ortles ice cores, the Tyrolean Iceman and glaciation of the highest summit of South Tyrol since the Northern Hemisphere Climatic Optimum. *The Cryosphere* 10, 2779–2797. doi: 10.5194/tc-10-2779-2016

Gäggeler H, von Gunten HR, Rössler E, Oeschger H and Schotterer U (1983) ²¹⁰Pb-dating of cold Alpine firn/ice cores from Colle Gnifetti, Switzerland. *Journal of Glaciology* 29(101), 165–177. doi: 10.3189/S0022143000005220

Gagliardini O and Meyssonnier J (1997) Flow simulation of a firn-covered cold glacier. *Annals of Glaciology* 24, 242–248. doi: 10.3189/S0260305500012246

Galibert G (1960a) Les processus actuels d'évolution du relief de Haute Montagne dans le massif de Zermatt (Alpes Valaisannes). *Bulletin de l'Association de Géographes Français* 290–291, 70–86.

Galibert G (1960b) L'évolution actuelle des 'faces nord' de la haute montagne alpine dans le massif de Zermatt. *Revue Géographique des Pyrénées et du Sud-Ouest* 31(2), 133–163.

Galibert G (1965) *La Haute Montagne Alpine – L'évolution Actuelle des Formes Dans les Hauts Massifs des Alpes et Dans Certains Reliefs de Comparaison.* Toulouse: Imp. F. Boisseau, 405 p.

Gardent M, Rabatel A, Dedieu J-P and Deline P (2014) Multitemporal glacier inventory of the French Alps from the late 1960s to the late 2000s. *Global and Planetary Change* 120, 24–37. doi: 10.1016/j.gloplacha.2014.05.004

Gilbert A, Vincent C, Gagliardini O, Krug J and Berthier E (2015) Assessment of thermal change in cold avalanching glaciers in relation to climate warming. *Geophysical Research Letters* 42(15), 6382–6390. doi: 10.1002/2015GL064838

Gilbert A, Vincent C, Wagnon P, Thibert E and Rabatel A (2012) The influence of snow cover thickness on the thermal regime of Tête Rousse Glacier (Mont Blanc range, 3200 m a.s.l.): consequences for outburst flood hazards and glacier response to climate change. *Journal of Geophysical Research: Earth Surface* 117, F002258. doi: 10.1029/2011JF002258

Gruber S and Haeberli W (2007) Permafrost in steep bedrock slopes and its temperature-related destabilization following climate change. *Journal of Geophysical Research* 112, F00547. doi: 10.1029/2006JF000547

Guillet G, Guillet T and Ravanel L (2020) Camera orientation, calibration and inverse perspective with uncertainties: a Bayesian method applied to area estimation from diverse photographs. *ISPRS Journal of Photogrammetry and Remote Sensing* 159, 237–255. doi: 10.1016/j.isprsjprs.2019.11.013

Guillet G, Preunkert S, Ravanel L, Montagnat S and Friedrich R (2021) Investigation of a cold-based ice apron on a high-mountain permafrost rock wall using ice texture analysis and micro-¹⁴C dating: a case study of the Triangle du Tacul ice apron (Mont Blanc massif, France). *Journal of Glaciology* 67(266), 1205–1212. doi: 10.1017/jog.2021.65

Guillet G and Ravanel L (2020) Variations in surface area of six ice aprons in the Mont-Blanc massif since the Little Ice Age. *Journal of Glaciology* 66(259), 777–789. doi: 10.1017/jog.2020.46

Haeberli W (1975) *Untersuchung zur Verbreitung von Permafrost zwischen Flüelapass und Piz Grialetsch (Graubünden)* (Dissertation der Universität Basel). Mitteilung VAW/ETHZ, 17, 221 p.

Haeberli W and 7 others and others (2006) Permafrost creep and rock glacier dynamics. *Permafrost and Periglacial Processes* 17(3), 189–214. doi: 10.1002/ppp.561

Haeberli W, Frauenfelder R, Kääb A and Wagner S (2004) Characteristics and potential climatic significance of 'miniature ice caps' (crest- and cornice-type low altitude ice archives). *Journal of Glaciology* 50(168), 129–136. doi: 10.3189/172756504781830330

Haeberli W and Funk M (1991) Borehole temperatures at the Colle Gnifetti core drilling site (Monte Rosa, Swiss Alps). *Journal of Glaciology* 37(125), 37–46. doi: 10.3189/S0022143000042775

Haeberli W and Gruber S (2009) Global warming and mountain permafrost. In Margesin R (ed). *Permafrost Soils.* Berlin, Heidelberg: Springer pp. 205–218. doi: 10.1007/978-3-540-69371-0_14

Haeberli W, Schmid W and Wagenbach D (1988) On the geometry, flow and age of firn and ice at the Colle Gnifetti core drilling site (Monte Rosa, Swiss Alps). *Zeitschrift für Gletscherkunde und Glazialgeologie* 24(1), 1–19.

Haeberli W, Wegmann M and Vonder Mühll D (1997) Slope stability problems related to glacier shrinkage and permafrost degradation in the Alps. *Eclogae Geologicae Helvetiae* 90, 407–414. doi: 10.5169/seals-168172

Harris C and 6 others and others (2009) Permafrost and climate in Europe: monitoring and modelling thermal, geomorphological and geotechnical responses. *Earth-Science Reviews* 92(3), 117–171. doi: 10.1016/j.earscirev.2008.12.002

Hartmeyer I and 6 others (2020) Current glacier recession causes significant rockfall increase: the immediate paraglacial response of deglaciating cirque walls. *Earth Surface Dynamics* 8, 729–751. doi: 10.5194/esurf-8-729-2020

Hasler A, Gruber S, Font M and Dubois A (2011) Advective heat transport in frozen rock clefts: conceptual model, laboratory experiments and numerical simulation. *Permafrost and Periglacial Processes* 22(4), 378–389. doi: 10.1002/ppp.737

Heucke E (2003) A light portable steam-driven ice drill suitable for drilling holes in ice and firn. *Geografiska Annaler: Series A, Physical Geography* 81, 603–609. doi: 10.1111/1468-0459.00088

Hoffmann H and 6 others (2018) A new sample preparation system for micro-¹⁴C dating of glacier ice with a first application to a high alpine ice core from Colle Gnifetti (Switzerland). *Radiocarbon* 60(2), 517–533. doi: 10.1017/RDC.2017.99

Hudleston PJ (1977) Progressive deformation and development of fabric across zones of shear in glacial ice. In Saxena SK, Bhattacharji S, Annersten H and Stephansson O (eds). *Energetics of Geological Processes.* Berlin Heidelberg: Springer, pp. 121–150.

Hudleston PJ (2015) Structures and fabrics in glacial ice: a review. *Journal of Structural Geology* 1, 1–27. doi: 10.1016/j.jsg.2015.09.003

Hugonnet R and 10 others (2021) Accelerated global glacier mass loss in the early twenty-first century. *Nature* 592, 726–731. doi: 10.1038/s41586-021-03436-z

IGN (2017) *Chamonix-Mont-Blanc – Massif du Mont Blanc – 3630 OT.* Map TOP25 Série bleue 1:25,000, EAN: 9782758540083.

Jenk TM and 9 others (2009) A novel radiocarbon dating technique applied to an ice core from the Alps indicating late Pleistocene ages. *Journal of Geophysical Research: Atmospheres* 114(D14), D011860. doi: 10.1029/2009JD011860

Journaux B (2019) Recrystallization processes, microstructure and crystallographic preferred orientation evolution in polycrystalline ice during high-temperature simple shear. *The Cryosphere* 13(5), 1495–1511. doi: 10.5194/tc-13-1495-2019

Kaushik S and 5 others (2021) Distribution and evolution of ice aprons in a changing climate in the Mont Blanc massif (western European Alps). *The International Archives of the Photogrammetry, Remote Sensing and Spatial Information Sciences*, XLIII-B3-2021, pp. 469–475. doi: 10.5194/isprs-archives-XLIII-B3-2021-469-2021

Kaushik S and 5 others (2022b) Effects of topographic and meteorological parameters on the surface area loss of ice aprons in the Mont Blanc massif (European Alps). *The Cryosphere* 16, 4251–4271. doi: 10.5194/tc-16-4251-2022

Kaushik S and 6 others (2022c) Analysis of the temporal evolution of ice aprons in the Mont-Blanc massif using X and C-band SAR images. *Frontiers in Remote Sensing* 3, 930021. doi: 10.3389/frsen.2022.930021

Kaushik S, Ravanel L, Magnin F, Trouvé E and Yan Y (2022a) Ice aprons in the Mont-Blanc massif (western European Alps): topographic characteristics and relations with glaciers and other types of perennial surface ice features. *Remote Sensing* 14, 5557. doi: 10.3390/rs14215557

Kaushik S, Ravanel L, Magnin F, Yan Y, Trouve E Cusicanqui D (2022b) Effects of topographic and meteorological parameters on the surface area loss of ice aprons in the Mont Blanc massif (European Alps). *The Cryosphere* 16, 4251–4271. doi: 10.5194/tc-16-4251-2022

Kenner R, Arenson LU and Grämiger L (2022) Mass movement processes related to permafrost and glaciation. In Shroder JF (ed.), *Treatise on*

Geomorphology, 2nd Edn., Amsterdam: Academic Press, Elsevier, 5, pp. 283–303. doi: 10.1016/B978-0-12-818234-5.00112-7

Krautblatter M, Funk D and Günzel FK (2013) Why permafrost rocks become unstable: a rock–ice-mechanical model in time and space. *Earth Surface Processes and Landforms* **38**(8), 876–887. doi: 10.1002/esp.3374

Legay A, Magnin F and Ravanel L (2021) Rock temperature prior to failure: analysis of 209 rockfall events in the Mont-Blanc massif (western European Alps). *Permafrost and Periglacial Processes* **32**(3), 520–536. doi: 10.1002/ppp.2110

Le Meur E and Vincent C (2006) Monitoring of the Taconnaz ice fall (French Alps) using measurements of mass balance, surface velocities and ice cliff position. *Cold Regions Science and Technology* **46**(1), 1–11. doi: 10.1016/j.coldregions.2006.05.001

Lliboutry L, Briat M, Creseveur M and Pourchet M (1976) 15 m deep temperatures in the glaciers of Mont Blanc (French Alps). *Journal of Glaciology* **16**(74), 197–203. doi: 10.3189/S0022143000031531

Lüthi M and Funk M (2000) Dating ice cores from a high Alpine glacier with a flow model for cold firn. *Annals of Glaciology* **31**, 69–79. doi: 10.3189/172756400781820381

Lüthi MP and Funk M (2001) Modelling heat flow in a cold, high-altitude glacier: interpretation of measurements from Colle Gnifetti, Swiss Alps. *Journal of Glaciology* **47**(157), 314–324. doi: 10.3189/172756501781832223

MacDonell S, Kinnard C, Mölg T, Nicholson L and Abermann J (2013) Meteorological drivers of ablation processes on a cold glacier in the semi-arid Andes of Chile. *The Cryosphere* **7**(5), 1513–1526. doi: 10.5194/tc-7-1513-2013

Magnin F and 5 others (2017) Snow control on active layer thickness in steep alpine rock walls (Aiguille du Midi, 3842 m a.s.l., Mont Blanc massif). *Catena* **149**, 648–662. doi: 10.1016/j.catena.2016.06.006

Magnin F, Brenning A, Bodin X, Deline P and Ravanel L (2015a) Statistical modelling of rock wall permafrost distribution: application to the Mont Blanc massif. *Géomorphologie* **21**, 145–162. doi: 10.4000/geomorphologie.10965

Magnin F, Deline P, Ravanel L, Noetzli J and Pogliotti P (2015b) Thermal characteristics of permafrost in the steep alpine rock walls of the Aiguille du Midi (Mont Blanc massif, 3842 m a.s.l). *The Cryosphere* **9**, 109–121. doi: 10.5194/tc-9-109-2015

Mamot P, Weber S, Schröder T and Krautblatter M (2018) A temperature- and stress-controlled failure criterion for ice-filled permafrost rock joints. *The Cryosphere* **12**, 3333–3353. doi: 10.5194/tc-12-3333-2018

Margreth S and 5 others (2011) Safety concept for hazards caused by ice avalanches from the Whymper Hanging Glacier in the Mont Blanc massif. *Cold Regions Science and Technology* **69**(2), 194–201. doi: 10.1016/j.coldregions.2011.03.006

Montagnat M and 6 others (2010) Waterfall ice: formation, structure and evolution. *Journal of Glaciology* **56**(196), 225–234. doi: 10.3189/002214310791968412

Moreau M (2010) Visual perception of changes in a high mountain landscape: the case of the retreat of the Évettes Glacier (Haute-Maurienne, northern French Alps). *Géomorphologie: Relief, Processus, Environnement* **16**(2), 165–174. doi: 10.4000/geomorphologie.7901

Mourey J, Marcuzzi M, Ravanel L and Pallandre F (2019) Effects of climate change on high Alpine mountain environments: evolution of mountaineering routes in the Mont Blanc massif (western Alps) over half a century. *Arctic, Antarctic, and Alpine Research* **51**(1), 176–189. doi: 10.1080/15230430.2019.1612216

Mourey J, Perrin-Malterre C and Ravanel L (2020) Strategies used by French Alpine guides to adapt to the effects of climate change. *Journal of Outdoor Recreation and Tourism* **29**, 100278. doi: 10.1016/j.jort.2020.100278

Noetzli J, Gruber S, Kohl T, Salzmann N and Haeberli W (2007) Three-dimensional distribution and evolution of permafrost temperatures in idealized high-mountain topography. *Journal of Geophysical Research – Earth Surface* **112**(F2), F000545. doi: 10.1029/2006JF000545

Paul F and 5 others and others (2013) On the accuracy of glacier outlines derived from remote-sensing data. *Annals of Glaciology* **54**, 171–182. doi: 10.3189/2013AoG63A296

Paul F, Frey H and Bris RL (2011) A new glacier inventory for the European Alps from Landsat™ scenes of 2003: challenges and results. *Annals of Glaciology* **52**(59), 144–152. doi: 10.3189/172756411799096295

PERMOS (2019) Permafrost in Switzerland 2014/2015 to 2017/2018. In Noetzli J, Pellet C and Staub B (eds). *Glaciological Report (Permafrost) n° 16–19 of the Cryospheric Commission of the Swiss Academy of Sciences.*

Fribourg: University of Fribourg, 104 pp. doi: 10.13093/permos-rep-2019-16-19

Pogliotti P and 6 others (2015) Warming permafrost and active layer variability at Cime Bianche, western European Alps. *The Cryosphere* **9**, 647–661. doi: 10.5194/tc-9-647-2015

Pourchet M, Debonnet E, Preiss N and Vincent C (1998) Le ^{7}Be: une aide à l'estimation des précipitations annuelles sur les glaciers froids. *Comptes Rendus de l'Académie des Sciences – Series IIA – Earth and Planetary Science* **327**(11), 721–725. doi: 10.1016/S1251-8050(99)80041-X

Pralong A and Funk M (2006) On the instability of avalanching glaciers. *Journal of Glaciology* **52**(176), 31–48. doi: 10.3189/172756506781828980

Preunkert S and 5 others (2019a) The Elbrus (Caucasus, Russia) ice core record – part 1: reconstruction of past anthropogenic sulfur emissions in south-eastern Europe. *Atmospheric Chemistry and Physics* **19**(22), 14119–14132. doi: 10.5194/acp-19-14119-2019

Preunkert S and 5 others and others (2019b) Lead and antimony in basal ice from Col du Dôme (French Alps) dated with radiocarbon: a record of pollution during antiquity. *Geophysical Research Letters* **46**(9), 4953–4961. doi: 10.1029/2019GL082641

Rabatel A, Letréguilly A, Dedieu J-P and Eckert N (2013) Changes in glacier equilibrium-line altitude in the western Alps from 1984 to 2010: evaluation by remote sensing and modeling of the morpho-topographic and climate controls. *The Cryosphere* **7**, 1455–1471. doi: 10.5194/tc-7-1455-2013

Raffestin C (2001) Les Alpes entre mythes et réalités. *Revue de Géographie Alpine* **89**(4), 13–26. doi: 10.3406/rga.2001.3055

Ravanel L and 5 others and others (2017b) Instrumentation thermique et cinématique des parois à permafrost du massif du Mont Blanc. *Collection EDYTEM* **19**, 27–38.

Ravanel L and Deline P (2011) Climate influence on rockfalls in high-Alpine steep rockwalls: the north side of the Aiguilles de Chamonix (Mont Blanc massif) since the end of the Little Ice Age. *The Holocene* **21**, 357–365. doi: 10.1177/0959683610374887

Ravanel L and Deline P (2013) A network of observers in the Mont Blanc massif to study rockfalls from high alpine rockwalls. *Geografia Fisica e Dinamica Quaternaria* **36**, 151–158. doi: 10.4461/GFDQ.2013.36.12

Ravanel L, Magnin F and Deline P (2017a) Impacts of the 2003 and 2015 summer heat waves on permafrost-affected rockwalls in the Mont Blanc massif. *Science of the Total Environment* **609**, 132–143. doi: 10.1016/j.scitotenv.2017.07.055

Rebuffat G (1973) *Le massif du Mont-Blanc – Les 100 plus belles courses.* Paris: Denoël, 238 pp.

Réveillet M and 6 others (2021) Spatio-temporal variability of surface mass balance in the accumulation zone of the Mer de Glace, French Alps, from multitemporal terrestrial LiDAR measurements. *Journal of Glaciology* **67**(261), 137–146. doi: 10.1017/jog.2020.92

Roe GH, Baker MB and Herla F (2017) Centennial glacier retreat as categorical evidence of regional climate change. *Nature Geoscience* **10**(2), 95–99. doi: 10.1038/ngeo2863

Schwarz J and 5 others and others (1981) Standardized testing methods for measuring mechanical properties of ice. *Cold Regions Science and Technology* **4**(3), 245–253. doi: 10.1016/0165-232X(81)90007-0

Schweizer J (1988) *Numerische Analyse Eine Hängegletschers am Lyskamm (Walliser Alpen).* Mitteilung: Versuchsanstalt für Wasserbau, Hydrologie und Glaziologie an der ETZH Zürich, 94, pp. 371–386.

Six D and Vincent C (2014) Sensitivity of mass balance and equilibrium-line altitude to climate change in the French Alps. *Journal of Glaciology* **60**(223), 867–878. doi: 10.3189/2014JoG14J014

Suter S and Hoelzle M (2002) Cold firn in the Mont Blanc and Monte Rosa areas, European Alps: spatial distribution and statistical models. *Annals of Glaciology* **35**, 9–18. doi: 10.3189/172756402781817059

Suter S, Laternser M, Haeberli W, Frauenfelder R and Hoelzle M (2001) Cold firn and ice of high-altitude glaciers in the Alps: measurements and distribution modelling. *Journal of Glaciology* **47**(156), 85–96. doi: 10.3189/172756501781832566

Thorsteinsson T, Kipfstuhl J and Miller H (1996) Textures and fabrics in the GRIP ice core. *Journal of Geophysical Research: Oceans* **102**, 26583–26599. doi: 10.1029/97JC00161

Uglietti C and 6 others (2016) Radiocarbon dating of glacier ice: overview, optimization, validation and potential. *The Cryosphere* **10**(6), 3091–3105. doi: 10.5194/tc-10-3091-2016

Vallon M, Vincent C and Reynaud L (1998) Altitudinal gradient of mass-balance sensitivity to climatic change from 18 years of observations on

glacier d'Argentière, France. *Journal of Glaciology* **44**(146), 93–96. doi: 10.3189/S0022143000002380

Vernier F and 6 others (2011) Fast correlation technique for glacier flow monitoring by digital camera and space-borne SAR images. *EURASIP Journal on Image and Video Processing* **2011**(1), 11. doi: 10.1186/1687-5281-2011-11

Vincent C (2002) Influence of climate change over the 20th century on four French glacier mass balances. *Journal of Geophysical Research - Atmospheres* **107**(D19), ACL 4-1–ACL 4-12. doi: 10.1029/2001JD000832

Vincent C and 5 others (2007a) Climate warming revealed by englacial temperatures at Col du Dôme (4250 m, Mont Blanc area). *Geophysical Research Letters* **34**, L16502. doi: 10.1029/2007GL029933

Vincent C and 5 others (2007b) Very high-elevation Mont Blanc glaciated areas not affected by the 20th century climate change. *Journal of Geophysical Research – Atmospheres* **112**, D09120. doi: 10.1029/2006JD007407

Vincent C and 9 others (2020) Strong changes in englacial temperatures despite insignificant changes in ice thickness at Dôme du Goûter glacier (Mont Blanc area). *The Cryosphere* **14**, 925–934. doi: 10.5194/tc-14-925-2020

Vincent C, Soruco A, Six D and Le Meur E (2009) Glacier thickening and decay analysis from 50 years of glaciological observations performed on Glacier d'Argentière, Mont Blanc area, France. *Annals of Glaciology* **50** (50), 73–79. doi: 10.3189/172756409787769500

Waller RI (2001) The influence of basal processes on the dynamic behaviour of cold-based glaciers. *Quaternary International* **86**(1), 117–128. doi: 10.1016/S1040-6182(01)00054-4

Wegmann M, Gudmundsson GH and Haeberli W (1998) Permafrost changes in rock walls and the retreat of alpine glaciers: a thermal modelling approach. *Permafrost and Periglacial Processes* **9**(1), 23–33. doi: 10.1002/(SICI)1099-1530(199801/03)9:1<23::AID-PPP274>3.0.CO;2-Y

Weiss J and 5 others (2002) Dome Concordia ice microstructure: impurities effect on grain growth. *Annals of Glaciology* **35**, 552–558. doi: 10.3189/172756402781816573

WGMS (1989) World Glacier Inventory – status 1988. In Haeberli W, Bösch H, Scherler K, Østrem G and Wallén CC. Zurich, Switzerland: *IAHS (ICSI)/UNEP/UNESCO*, World Glacier Monitoring Service, 458 pp.

Wilson C, Russell-Head D and Sim H (2003) The application of an automated fabric analyzer system to the textural evolution of folded ice layers in shear zones. *Annals of Glaciology* **37**, 7–17. doi: 10.3189/172756403781815401

Zampieri M and 5 others (2016) Global assessment of heat wave magnitudes from 1901 to 2010 and implications for the river discharge of the Alps. *Science of the Total Environment* **571**, 1330–1339. doi: 10.1016/j.scitotenv.2016.07.008

Zipf L, Merchel S, Bohleber P, Rugel G and Scharf A (2016) Exploring ice core drilling chips from a cold Alpine glacier for cosmogenic radionuclide (^{10}Be) analysis. *Results in Physics* **6**, 78–79. doi: 10.1016/j.rinp.2016.01.002

Zoller H, Schindler C and Röthlisberger F (1966) Postglaziale gletscherstande und klimaschwankungen im Gotthardmassiv und Vorderheingebiet. *Verhandlungen der Naturforschenden Gesellschaft in Basel* **77**, 97–164.